Endothelial adhesion receptors are recruited to adherent leukocytes by inclusion in preformed tetraspanin nanoplatforms

Olga Barreiro,[1,2] Moreno Zamai,[4,5] María Yáñez-Mó,[1,2] Emilio Tejera,[1,2] Pedro López-Romero,[3] Peter N. Monk,[6] Enrico Gratton,[7] Valeria R. Caiolfa,[2,4,5] and Francisco Sánchez-Madrid[1,2]

[1]Servicio de Inmunología, Hospital de la Princesa, Universidad Autónoma de Madrid, 28006 Madrid, Spain
[2]Departamento de Biología Vascular e Inflamación and [3]Unidad de Genómica, Centro Nacional de Investigaciones Cardiovasculares, 28029 Madrid, Spain
[4]Department of Molecular Biology and Functional Genomics and [5]Italian Institute of Technology Network Research, Unit of Molecular Neuroscience, San Raffaele Scientific Institute, 20132 Milan, Italy
[6]Academic Neurology Unit, School of Medicine and Biomedical Science, University of Sheffield, Sheffield S10 2RX, England, UK
[7]Laboratory for Fluorescence Dynamics, Biomedical Engineering Department, University of California, Irvine, Irvine, CA 92697

VCAM-1 and ICAM-1, receptors for leukocyte integrins, are recruited to cell–cell contact sites on the apical membrane of activated endothelial cells. In this study, we show that this recruitment is independent of ligand engagement, actin cytoskeleton anchorage, and heterodimer formation. Instead, VCAM-1 and ICAM-1 are recruited by inclusion within specialized preformed tetraspanin-enriched microdomains, which act as endothelial adhesive platforms (EAPs). Using advanced analytical fluorescence techniques, we have characterized the diffusion properties at the single-molecule level, nanoscale organization, and specific intradomain molecular interactions of EAPs in living primary endothelial cells. This study provides compelling evidence for the existence of EAPs as physical entities at the plasma membrane, distinct from lipid rafts. Scanning electron microscopy of immunogold-labeled samples treated with a specific tetraspanin-blocking peptide identify nanoclustering of VCAM-1 and ICAM-1 within EAPs as a novel mechanism for supramolecular organization that regulates the leukocyte integrin–binding capacity of both endothelial receptors during extravasation.

Introduction

How cells physically organize and compartmentalize receptors and signaling molecules into specialized, efficient, regulated networks is of critical importance to our understanding of the complexity and dynamics of biological processes. In this regard, cholesterol and sphingolipid-enriched rafts have been proposed as platforms for the sorting of specific membrane components, such as glycosylphosphatidylinositol (GPI)-anchored proteins, and as sites for the assembly of cytoplasmic signaling complexes (Simons and Toomre, 2000; Anderson and Jacobson, 2002). Recent biochemical, proteomic, and structural studies bolster the idea that tetraspanin-enriched microdomains (TEMs) at the plasma membrane play a key role in organizing molecular complexes with protein compositions different from those of typical lipid rafts (Hemler, 2005; Le Naour et al., 2006; Min et al., 2006). The existence and physical properties of lipid rafts have been extensively studied by innovative analytical methods (Kenworthy et al., 2004; Sharma et al., 2004; Larson et al., 2005; Suzuki et al., 2007). However, the presence and molecular dynamics of TEMs on the plasma membrane of living cells have not been explored.

Tetraspanins are ubiquitous, low molecular weight proteins that span the plasma membrane four times and are able to organize themselves by homo- and heterooligomerization (Hemler, 2005). Moreover, these molecules can simultaneously associate laterally

Correspondence to Francisco Sánchez-Madrid: fsanchez.hlpr@salud.madrid.org

Abbreviations used in this paper: ACF, autocorrelation function; EAP, endothelial adhesive platform; FCS, fluorescence correlation spectroscopy; FLIM, fluorescence lifetime imaging microscopy; FN, fibronectin; FRET, Förster resonance energy transfer; FRETeff, FRET efficiency; GPI, glycosylphosphatidylinositol; HUVEC, human umbilical vein endothelial cell; knn, k nearest neighbor; LEL, large extracellular loop; mEGFP, monomeric EGFP; TEM, tetraspanin-enriched microdomain; VE-cadherin, vascular endothelial cadherin.

The online version of this article contains supplemental material.

The Rockefeller University Press $30.00
J. Cell Biol. Vol. 183 No. 3 527–542
www.jcb.org/cgi/doi/10.1083/jcb.200805076

at the plasma membrane with numerous integral membrane receptors, modulating their functions and organizing discrete, dynamic plasma membrane compartments. These partners include integrins and other adhesion molecules (Yanez-Mo et al., 1998; Berditchevski, 2001; Barreiro et al., 2005), CD19–CD21 (Cherukuri et al., 2004; Levy and Shoham, 2005), major histocompatibility complex–peptide complexes (Kropshofer et al., 2002), Fc receptors (Moseley, 2005), G protein–coupled receptors (Little et al., 2004), and metalloproteinases (Yan et al., 2002). Tetraspanins also associate intracellularly with several cytoplasmic signaling mediators such as type II PI4K or PKC isoforms (Yauch and Hemler, 2000; Zhang et al., 2001). Apart from acting as adapters for membrane organization, tetraspanins also regulate the trafficking and biosynthetic processing of associated receptors (Berditchevski and Odintsova, 2007). Although TEMs seem to be different from biochemically defined lipid rafts (Simons and Toomre, 2000), they are not devoid of lipid interactions because tetraspanins are highly palmitoylated proteins that bind cholesterol and gangliosides (Charrin et al., 2003; Yang et al., 2004).

The composition and other specific characteristics of TEMs may vary with cell type. Gene deletion, knockdown, overexpression, and mutation experiments have revealed key functional roles for tetraspanins in many fundamental physiological processes, among which are egg–sperm fusion (Le Naour et al., 2000; Miyado et al., 2000), antigen presentation (Kropshofer et al., 2002; Levy and Shoham, 2005; Unternaehrer et al., 2007), viral cell entry and budding and virus-promoted syncytia formation (Pileri et al., 1998; Gordon-Alonso et al., 2006; Nydegger et al., 2006), kidney failure and tissue angiogenesis (Sachs et al., 2006; Takeda et al., 2007), and cell adhesion, migration, and invasion (Yanez-Mo et al., 1998, 2008; Chattopadhyay et al., 2003; Hemler, 2003; Barreiro et al., 2005). Because there are few known tetraspanin ligands, it is very likely that these molecules exert their regulatory effects indirectly through their lateral binding to assorted partners. However, the molecular mechanisms underlying the regulatory activity of tetraspanins remain elusive.

Leukocyte extravasation from the bloodstream to sites of infection and inflammation involves a dynamic interaction with the endothelium that is mediated by an array of leukocyte and endothelial cell surface receptors. This process consists of sequential steps of tethering, rolling, firm adhesion, locomotion, and diapedesis, with specialized receptor/ligand pairs involved in each (Ley et al., 2007). Previous studies have shown that, to prevent leukocyte detachment under hemodynamic flow, endothelial cells form actin-based structures that cluster VCAM-1, ICAM-1 (Barreiro et al., 2002; Carman and Springer, 2003; van Buul et al., 2007), tetraspanins, and actin-binding proteins at the contact area with leukocytes (Barreiro et al., 2002, 2005).

In this study, we demonstrate that before leukocyte binding, the apical plasma membrane of living endothelial cells possesses specialized microdomains containing tetraspanins and adhesion receptors (VCAM-1 and ICAM-1), which we have termed endothelial adhesive platforms (EAPs). This particular kind of TEM promotes molecular aggregation at the nanoscopic scale (nanoclustering) of adhesion receptors to enhance their adhesive properties during leukocyte adhesion to endothelium. By using advanced analytical fluorescence microscopy techniques, we have determined the molecular characteristics, dynamics, and biophysical properties of EAPs. Finally, using scanning electron microscopy in combination with tetraspanin-blocking peptides, we show that tetraspanin microdomains make an essential contribution to the avidity regulation of endothelial adhesion receptors, fine-tuning their adhesive properties.

Results

Endothelial ICAM-1 and VCAM-1 cluster at the docking structure independently of counterreceptor engagement and actin anchorage

We have previously shown that at contact sites with adherent leukocytes, activated endothelial cells form three-dimensional actin-based docking structures that cluster VCAM-1 and ICAM-1 (Barreiro et al., 2002). To analyze the dynamic recruitment of adhesion molecules to these docking structures, we induced their formation with K562 cells expressing either $\alpha4\beta1$ or $\alpha L\beta2$ integrins (K562 $\alpha4$ or K562 lymphocyte function-associated antigen–1 [LFA-1]), which adhere to activated endothelial cells via VCAM-1 or ICAM-1, respectively. Surprisingly, both ICAM-1 and VCAM-1 clustered at the docking structure formed around either K562 clone, regardless of whether they were directly engaged by their corresponding integrin receptor (Fig. 1 A). To assess the generality of this corecruitment, we examined the docking structures formed with T lymphoblasts, which express both LFA-1 and very late antigen–4 (VLA-4); before adhesion to activated human umbilical vein endothelial cells (HUVECs), LFA-1 was blocked with a specific allosteric antagonist (BIRT377), or VLA-4 was blocked with a ligand-binding inhibitor (BIO5192). In both cases, VCAM-1 and ICAM-1 were corecruited in a similar way as observed with K562 cells (Fig. 1 B).

To assess the involvement of the endothelial actin cytoskeleton in VCAM-1–ICAM-1 corecruitment, we transiently transfected resting HUVECs with a cytoplasmic tail–truncated VCAM-1 mutant (VCAMΔCyt). Under these conditions, HUVECs bear low levels of ICAM-1 and negligible levels of endogenous VCAM-1. Upon engagement of VCAMΔCyt by K562 $\alpha4$, discrete clusters containing VCAMΔCyt and ICAM-1 were observed around adhered cells, but in no case was a well-developed three-dimensional structure formed (Fig. 1 C, i). In contrast, when ICAM-1 was directly engaged by K562 LFA-1, a proper docking structure was formed, also containing VCAMΔCyt (Fig. 1 C, ii). Likewise, well-formed docking structures containing ICAM-1 and VCAMΔCyt were induced by adhered T lymphoblasts (Fig. 1 C, iii). These data suggest that the engagement of one endothelial adhesion receptor by its corresponding leukocyte integrin corecruits the other receptor toward the contact area. This coclustering must involve the extracellular or transmembrane domains of both adhesion molecules because it occurs with cytoplasmic tail–truncated forms. However, subsequent reorganization of the endothelial actin cytoskeleton into the protrusive cup requires actin anchorage of the cytoplasmic tail of the ligand-bound endothelial adhesion molecule.

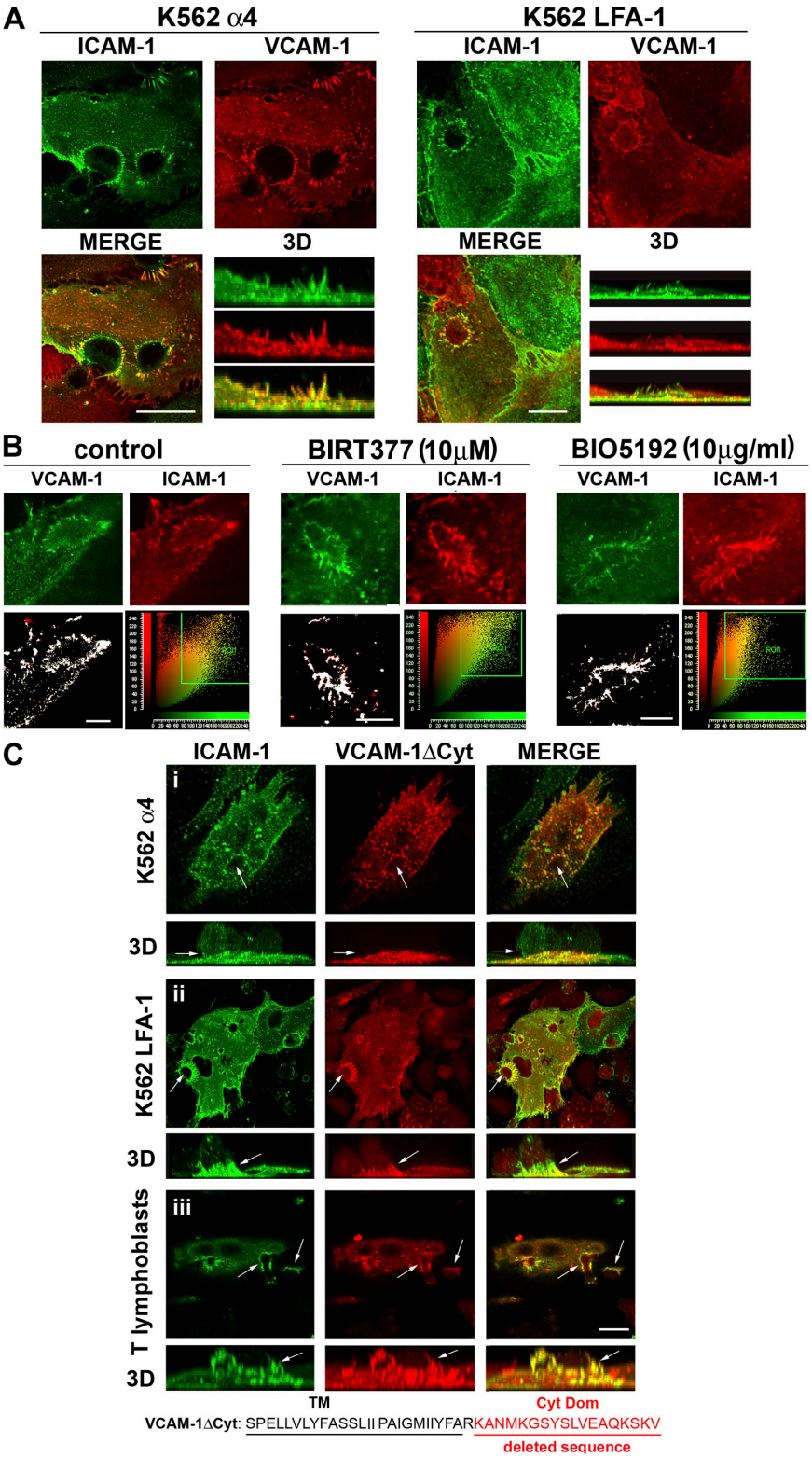

Figure 1. **VCAM-1 and ICAM-1 are copresented at lymphocyte–endothelium contact sites independently of ligand binding and actin anchorage.** (A) K562 α4 or LFA-1 was adhered (30 min) to TNF-α–activated HUVECs. Samples were fixed and double stained with anti–VCAM-1 (P8B1) and biotin-conjugated anti–ICAM-1 (MEM111). Confocal stacks were obtained, and orthogonal maximal projections and vertical three-dimensional reconstructions of the whole series are displayed. (B) Human T lymphoblasts were pretreated (5 min) with 10 μM BIRT377 or 10 μg/ml BIO5192 to inactivate LFA-1 or VLA-4 and were added to TNF-α–activated HUVECs for 5 min. Fixed cells were double stained as in A. Confocal stacks were obtained, and a representative section from each treatment is shown together with its corresponding colocalization histogram and a mask showing the distribution of double green-red pixels (marked regions) within the cell. (C) Resting HUVECs transfected with VCAMΔCyt were incubated with K562 α4 (i), K562 LFA-1 (ii), or T lymphoblasts (iii). Fixed cells were double stained with anti–VCAM-1 (VCAMΔCyt was the only VCAM-1 species detected) and biotin-conjugated anti–ICAM-1. Confocal stacks were obtained; representative sections or vertical reconstructions of the whole series are displayed. Arrows show positions of adhered leukocytes. The deleted sequence in the VCAMΔCyt construct is shown in red below the figure. TM, transmembrane; Cyt Dom, cytoplasmic domain. Bars: (A and C) 20 μm; (B) 10 μm.

Analysis of homo- and heterophilic interactions of ICAM-1 and VCAM-1 in living endothelial cells

Because cytoskeletal anchorage cannot account for adhesion receptor corecruitment, we investigated the potential formation of VCAM-1–ICAM-1 heterodimers at the apical membrane of living primary endothelial cells by Förster resonance energy transfer (FRET)–fluorescence lifetime imaging microscopy (FLIM) analysis. For this purpose, we generated functional VCAM-1 and ICAM-1 chimeras fused to monomeric EGFP (mEGFP) as donor and mRFP1 as acceptor. The constructs were transiently cotransfected into primary HUVECs under resting conditions to prevent up-regulation of endogenous VCAM-1 and ICAM-1 expression. We then analyzed the molecular interactions at a nanometric scale

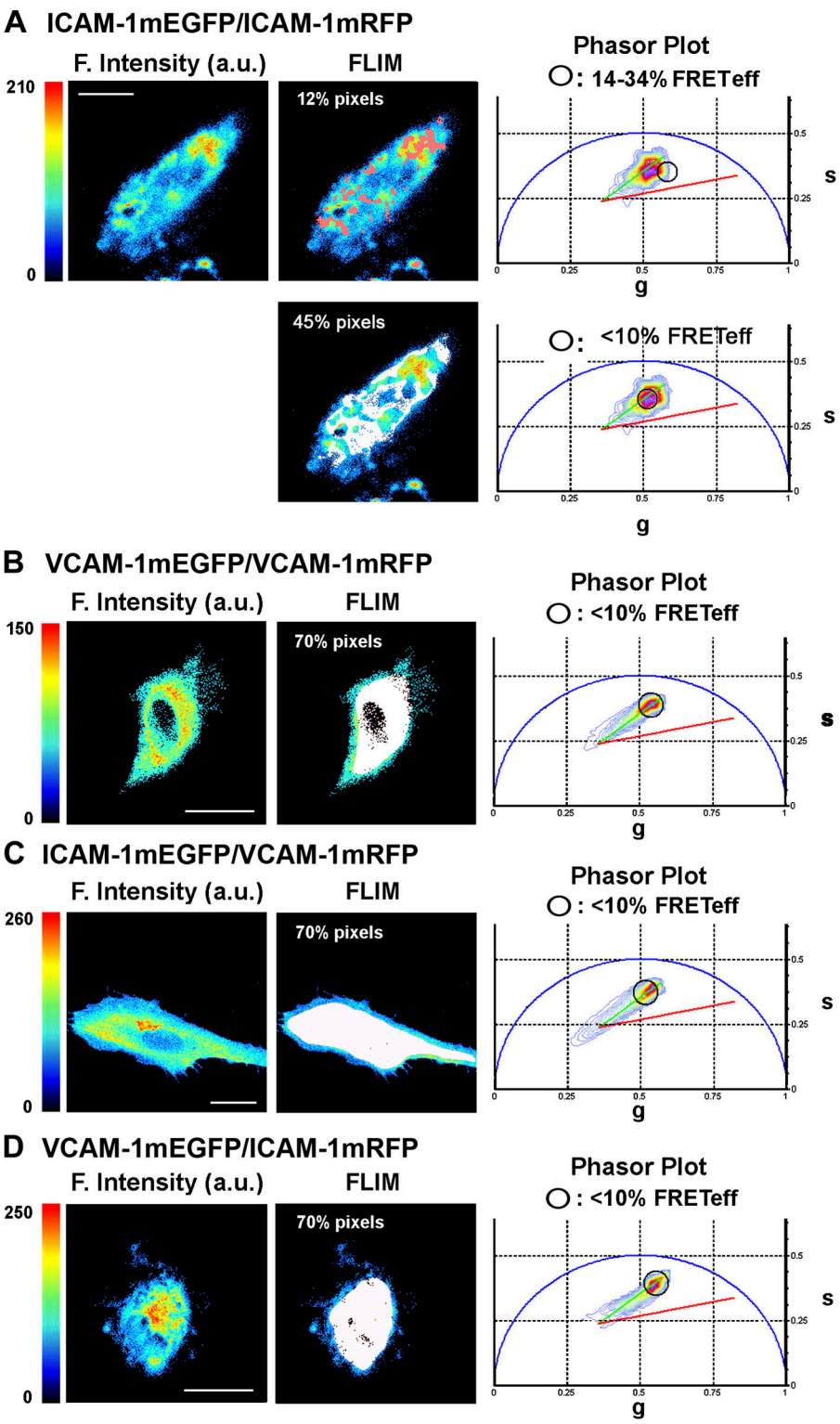

Figure 2. **VCAM-1 and ICAM-1 do not interact at the plasma membrane.** Endothelial cells were cotransfected with mEGFP–mRFP1 pairs (ICAM-1–ICAM-1, VCAM-1–VCAM-1, ICAM-1–VCAM-1, and VCAM-1–ICAM-1). A representative FRET–FLIM analysis using the phasor plot is shown for each pair. The sine (s) and cosine (g) transforms of the lifetime data measured in the frequency mode generate the coordinate system presented in the phasor (Digman et al., 2008). Fluorescence intensity (F. intensity) images are in pseudocolor (left), and corresponding mEGFP lifetime distributions are shown in the plots after the phasor transformation (right). In each phasor plot, the green line represents 0% FRETeff and the red line marks 50% FRETeff (Caiolfa et al., 2007). The black circular cursors in the phasor plots select the subset of pixels shown in the correlated FLIM images (pink mask for positive FRET and white mask for negative FRET; middle). For the ICAM-1–ICAM-1 pair (A), most pixels lie very close to the green line (FRETeff ≤10%; negligible), but 12% of pixels exhibit FRETeff of 14–34%. These positive pixels are localized in clusters, as shown by the FLIM image (pink mask). Other protein pairs (B–D) show phasor distributions indistinguishable from that of the negative controls (Fig. S1 A, available at http://www.jcb.org/cgi/content/full/jcb.200805076/DC1). a.u., arbitrary units. Bars, 20 µm.

between ICAM-1–ICAM-1, VCAM-1–VCAM-1, and ICAM-1–VCAM-1 by alternately using each receptor as donor (Fig. 2). The fluorescence lifetime of the donor in each cotransfection was compared with that of singly transfected ICAM-1– or VCAM-1–mEGFP (donor standards in Fig. S1 A, available at http://www.jcb.org/cgi/content/full/jcb.200805076/DC1). In the case of ICAM-1–ICAM-1 interaction, although most pixels were below the FRET detection threshold (FRET efficiency [FRETeff] ≤ 10%), the remaining pixels (12%) showed positive FRETeff of 14–34% and were localized in clusters at the membrane (Fig. 2 A). In contrast, the analysis showed no significant molecular interactions of the VCAM-1–VCAM-1, ICAM-1–VCAM-1, and VCAM-1–ICAM-1 pairs (Fig. 2, B–D). Thus, under these conditions, homophilic ICAM-1–ICAM-1 interactions, but not VCAM-1–VCAM-1 or heterophilic VCAM-1–ICAM-1 interactions, are detected on the plasma membrane of living primary endothelial cells.

Tetraspanin microdomains are involved in the formation of specialized EAPs

Because there is no heterophilic ICAM-1–VCAM-1 interaction, the coclustering of adhesion receptors may involve their lateral association with specific plasma membrane microdomains. We have previously found that the CD9, CD81, and CD151 tetraspanins concentrate at docking structures around primary human leukocytes and coprecipitate together with VCAM-1 and ICAM-1 (Barreiro et al., 2005). In this study, we found that tetraspanin proteins were also enriched at docking sites in the K562 α4 and LFA-1 adhesion models (Fig. S2 A, available at http://www.jcb.org/cgi/content/full/jcb.200805076/DC1). To examine this association further, we engaged endothelial surface proteins with specific magnetic bead–coated antibodies, finding that engagement of either CD9 or CD151 corecruited both ICAM-1 and VCAM-1. Conversely, beads coated with anti–VCAM-1 corecruited ICAM-1 and vice versa, and both antibodies clustered tetraspanins. In contrast, anti–vascular endothelial cadherin (VE-cadherin)–coated beads did not significantly recruit ICAM-1, VCAM-1, or tetraspanins above basal levels (Fig. S2, B and C; and not depicted).

Sucrose gradient fractionation of lysates of TNF-α–activated HUVECs showed that most tetraspanins are soluble under these conditions and migrate with the dense fractions (F1–F7) together with ICAM-1 and VCAM-1, which were not found in lipid raft fractions containing caveolin (Fig. S2 D). These results strongly suggest that endothelial tetraspanin microdomains containing VCAM-1 and ICAM-1 are distinct from classical biochemically defined lipid rafts and may constitute specialized, organized membrane structures, which we have termed EAPs.

Molecular dynamics at EAPs

To explore the molecular dynamics of tetraspanins and adhesion receptors at EAPs, we first used FRAP to study the diffusional properties of EGFP-tagged CD9, CD151, VCAM-1, and ICAM-1 at the nude apical plasma membrane of HUVECs in comparison with the lipid raft marker GPI-EGFP (Fig. 3 A and Table S1, available at http://www.jcb.org/cgi/content/full/jcb.200805076/DC1; Sharma et al., 2004). The derived apparent diffusion coefficient (Table S1) and the immobile fraction (1 − R) for each protein (Fig. 3 A) were calculated. GPI-EGFP showed the highest mobility (∼1 $\mu m^2/s$, as previously described in Kenworthy et al., 2004). Tetraspanins and ICAM-1 behaved similarly (D = ∼0.5 $\mu m^2/s$), whereas VCAM-1 seemed to diffuse slower (D = ∼0.3 $\mu m^2/s$) and exhibited a higher immobile fraction.

To assess the influence of leukocyte adhesion on EAP dynamics, FRAP was performed on endothelial docking structures induced by engagement of K562 α4 or LFA-1 (Fig. 3, B–D). The most notable effects were when an endothelial adhesion receptor was specifically bound to its ligand, a greater proportion of the protein population remained immobile, and the mobility of the residual mobile fraction was locally restricted (Fig. 3, C and D; and Fig. S3 A, available at http://www.jcb.org/cgi/content/full/jcb.200805076/DC1). Other nonligated EAP components were affected to a lesser extent, exhibiting a variable slowdown in FRAP recovery curves compared with analyses of the same molecules at other plasma membrane regions of similar size (Fig. S3 A). Statistical analyses showed that ICAM-1 engagement had the greater effect on CD9 mobility, whereas CD151 was more affected by VCAM-1 engagement (Table S2 and Fig. S3 A). These data thus suggest a degree of specificity among tetraspanin–partner interactions within EAPs. GPI-EGFP diffusion was not altered at docking structures (Fig. 3 E).

Differences in the diffusion of tetraspanins and adhesion receptors could be related to their differential anchorage to the actin cytoskeleton. We therefore analyzed the dynamics of a cytoplasmic tail–truncated mutant of ICAM-1 (ICAM-1ΔCyt-EGFP), which lacks actin–cytoskeleton linking activity. Freed of cytoskeletal constraints, this truncated ICAM-1 diffused at the plasma membrane more rapidly than the full-length receptor (Fig. S3 B). ICAM-1ΔCyt-EGFP also had a faster fluorescence recovery rate than the wild-type molecule at docking sites with K562 LFA-1 cells, indicating that stabilization of the ICAM-1–LFA-1 interaction also implies anchorage of ICAM-1 to the endothelial F-actin cytoskeleton (Fig. S3 B).

To accurately estimate the diffusional features of individual EAP components, we applied fluorescence correlation spectroscopy (FCS) to mEGFP-tagged ICAM-1, VCAM-1, CD9, and CD151 expressed in living primary human endothelial cells. The autocorrelation functions (ACFs) derived from fluorescence intensity traces were best fitted using an anomalous diffusion model. We found that all of these proteins showed a pattern of local diffusion confinement, with ICAM-1 and VCAM-1 showing slower overall diffusion than tetraspanins, correlating with a higher diffusion anomality (smaller α coefficient values; Fig. 4 A). Tetraspanins showed a higher relative frequency of faster diffusion than adhesion receptors (Fig. S4 A, available at http://www.jcb.org/cgi/content/full/jcb.200805076/DC1). This might indicate a more confined diffusion of VCAM-1 and ICAM-1 within EAPs versus a more dynamic exchange of tetraspanins among different microdomains. Furthermore, we found a pronounced decrease in the molecular mobility of CD9 within docking structures compared with nude plasma membrane (Fig. 4 B), concurring with data obtained by FRAP analysis.

Specificity of tetraspanin–adhesion receptor interactions within EAPs

Next, we performed additional FRET–FLIM analyses in living endothelial cells to explore the molecular interactions among CD9, CD151, ICAM-1, and VCAM-1. These assays confirmed the homophilic CD9–CD9 and heterophilic CD9–CD151 interactions (Fig. 5, A and B) previously shown by biochemical studies (for review see Hemler, 2005). In addition, we found that CD9 preferentially interacted with ICAM-1 and CD151 with VCAM-1, with FRETeff values close to those detected between tetraspanins (Fig. 5, C and D). In contrast, VCAM-1–CD9 and ICAM-1–CD151 interactions were scarce throughout the cell membrane and were not detected in all cells studied (Fig. S1, B and C). These results further support the existence of differential molecular interactions in EAPs and strongly suggest that there are preferential associations between specific adhesion receptors

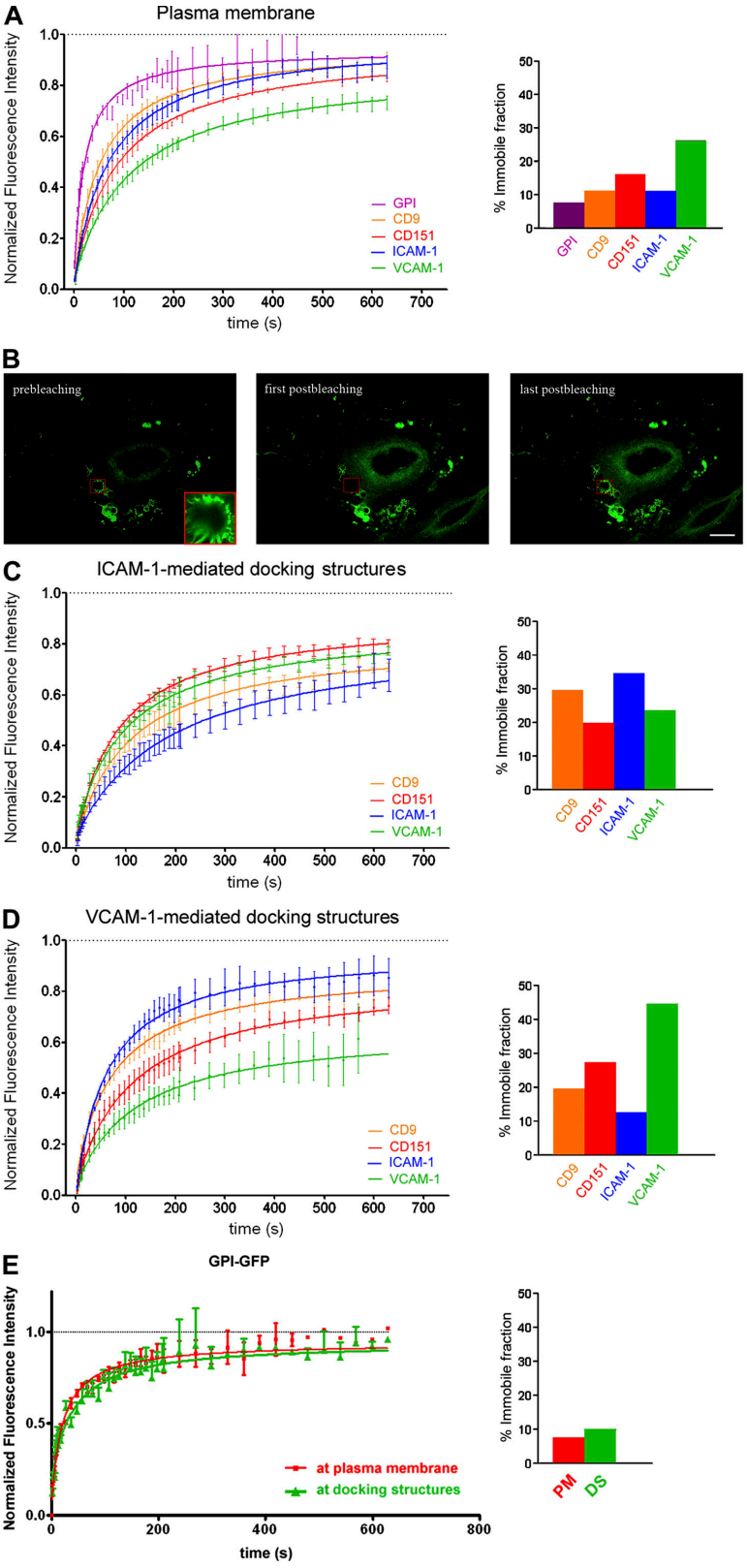

Figure 3. **EAP component dynamics at nude membrane and docking structures.** (A) Endothelial cells were transiently transfected with CD9-, CD151-, ICAM-1–, VCAM-1–, or GPI-EGFP and activated with TNF-α. FRAP curves from comparable areas of nude plasma membrane were acquired and fitted by a simple diffusion model. Mean-fitted fluorescence recovery curves ± SEM are depicted on the overlay graphic. (B) Representative FRAP analysis at an endothelial docking structure. Prebleaching image shows an ICAM-1–EGFP-transfected endothelial cell with docking structures formed around attached K562 LFA-1 cells (circles of high fluorescence). The boxed docking structure, shown in the inset at high magnification during bleaching, was selected for photobleaching recovery. Bar, 20 µm. (C and D) Mean-fitted fluorescence recovery curves ± SEM for ICAM-1–, VCAM-1–, CD9-, and CD151-EGFP at docking structures (comparable areas) formed around K562 LFA-1 or K562 α4. (E) Mean-fitted fluorescence recovery curves ± SEM for GPI-EGFP at plasma membrane (PM) or docking structures (DS; comparable areas). Immobile fractions calculated from fitted curves are shown in the bar histograms. Statistical analysis and number of experiments are shown in Table S2 (available at http://www.jcb.org/cgi/content/full/jcb.200805076/DC1).

and tetraspanins. In further biochemical and microscopy analyses, we searched for other endothelial receptors that might interact with tetraspanins and cluster at the leukocyte–endothelial contact area independently of ligand binding, identifying PECAM-1/CD31, CD44, JAM-A, and ICAM-2 as putative EAP components (Fig. S4, B and C; and not depicted). In contrast, VE-cadherin does not coprecipitate tetraspanins (Fig. S4 B), and its engagement does not induce corecruitment of EAP components (Fig. S2, B and C), suggesting its exclusion from these specialized membrane microdomains.

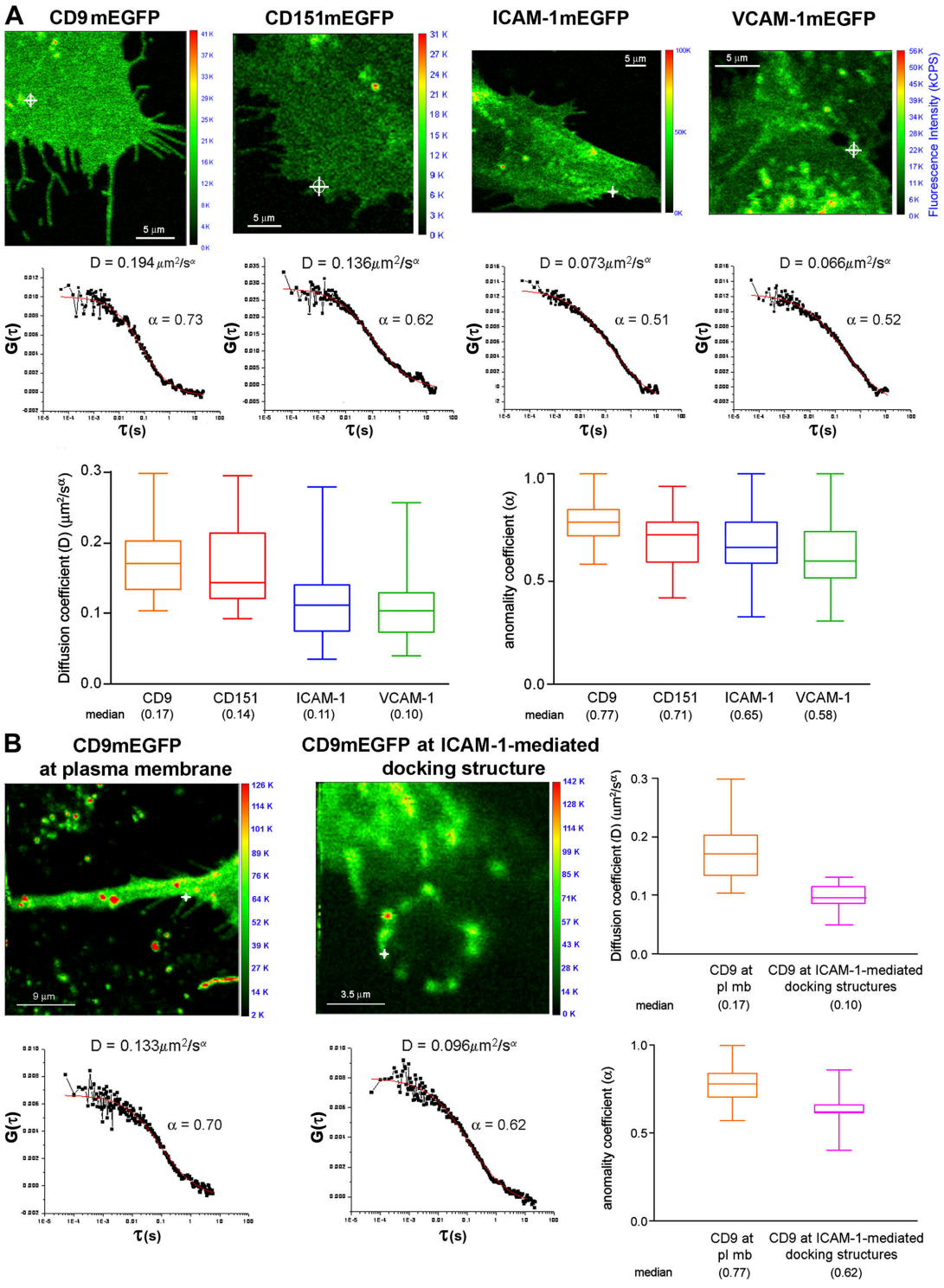

Figure 4. **EAP component diffusion at nude membrane and docking structures.** (A) Representative FCS measurements at plasma membranes of transiently transfected primary HUVECs expressing very low levels of CD9-, CD151-, ICAM-1–, or VCAM-1–mEGFP. For each condition, the figure shows the fluorescence intensity image (kCPS, kilo counts per second), the ACF (black line) derived from the fluorescence intensity trace acquired at the point marked with a white cross, the best-fitted curve using an anomalous diffusion model (red line), and the diffusion (D) and anomality (α) coefficients. In the FCS autocorrelation curves, the x axis (τ) represents the delay time in seconds, and the y axis (G(τ)) is the autocorrelation amplitude as a function of delay time. Box-whisker plots show distributions of D and α values obtained from several transiently transfected HUVEC batches using mEGFP and mRFP1 versions of the four proteins; minimum, 25th percentile, median, 75th percentile, and maximum values are shown. (B) Representative FCS measurements of CD9-mGFP at the plasma membrane and an endothelial ICAM-1–mediated docking structure formed around an adhered K562 LFA-1 cell. The same parameters described in A are shown. Box-whisker plots compare data from the plasma membrane (reproduced from A) with data from docking structures. Statistical analysis and number of experiments are reported in Table S3 (available at http://www.jcb.org/cgi/content/full/jcb.200805076/DC1).

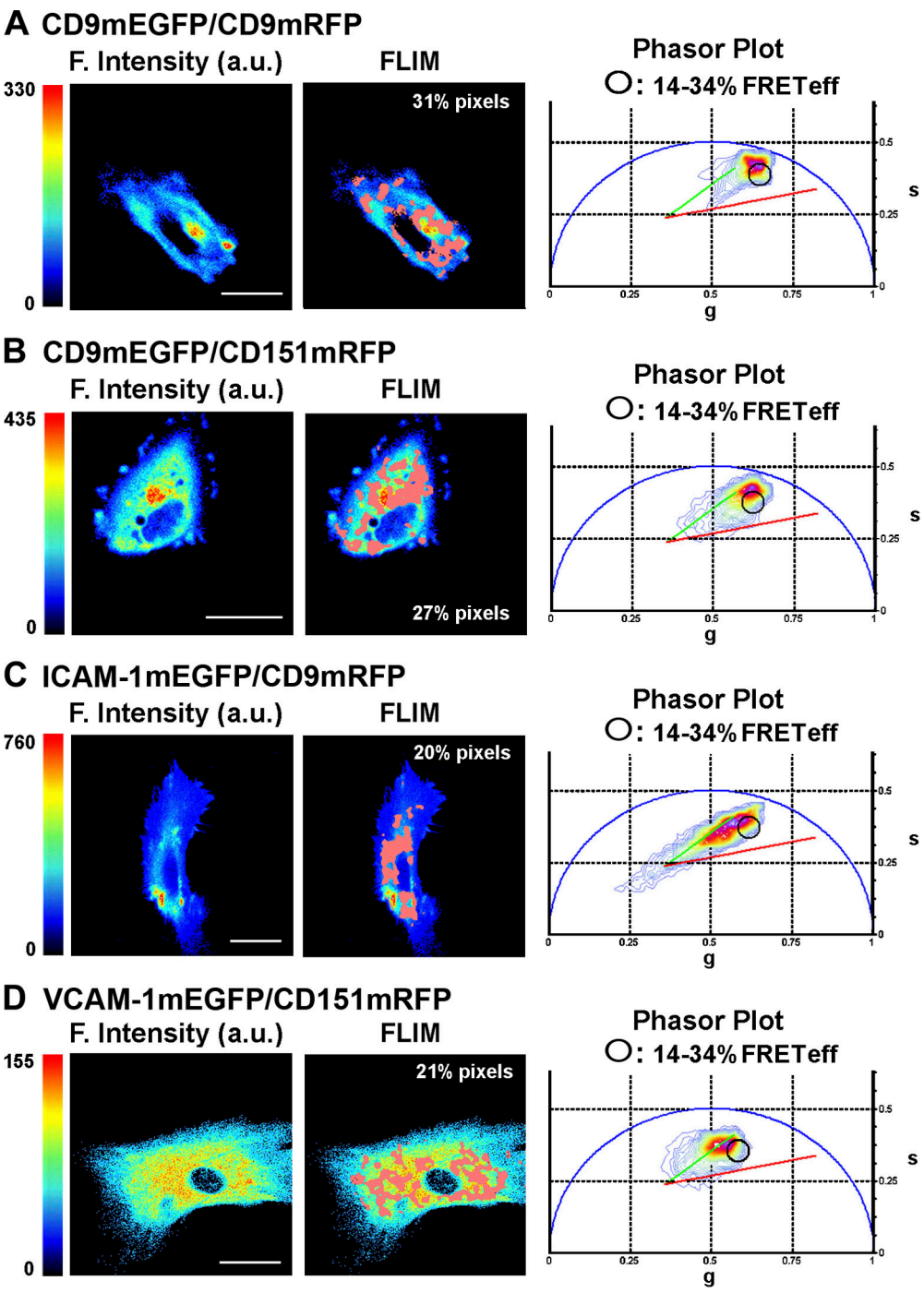

Figure 5. **Specificity of molecular interactions in EAP HUVECs transfected with mEGFP–mRFP1 pairs (CD9–CD9, CD9–CD151, ICAM-1–CD9, and VCAM-1–CD151).** FRET–FLIM analysis was performed as in Fig. 2. For each FRET pair, the figure shows the fluorescence intensity (F. intensity) image (in pseudo-color scale), the phasor plot, and the FLIM image corresponding to the cursor selection in phasors (black circles), with the location of the highest FRETeff population illustrated with the pink mask (14–34% FRETeff). a.u., arbitrary units; s, sine; g cosine. Bars, 20 µm.

Role of tetraspanins in the molecular dynamics and nanoclustering of adhesion receptors in EAPs

To investigate the role of tetraspanins in the molecular dynamics of EAPs, we used the tetraspanin-blocking peptide CD9–large extracellular loop (LEL)–GST. Tetraspanin-blocking peptides have been used to perturb functions regulated by tetraspanin microdomains, such as egg–sperm fusion, monocytic giant cell formation and HIV infection (Zhu et al., 2002; Takeda et al., 2003; Ho et al., 2006), and VCAM-1– and ICAM-1–mediated lymphocyte adhesion strength and transmigration under flow in vitro (Barreiro et al., 2005). However, the mechanism of action of LEL peptides has not been elucidated yet. FCS analyses showed that CD9-LEL-GST decreased the diffusion of CD9 and CD151 (Fig. 6, A–C), suggesting that interference with CD9, the most abundant EAP component, has a critical effect on EAP organization and dynamics.

The spatial organization of EAPs was assessed by scanning electron microscopy combined with immunogold labeling of VCAM-1 and ICAM-1. We found submicrometer-sized homo- and heteroclusters of these adhesion receptors throughout the nude apical plasma membrane (Fig. 7 A and Fig. 8, left), supporting the concept of preexistent EAP microdomains. Localized high density clustering was observed at the microvilli of docking structures around adherent leukocytes (shown for ICAM-1; Fig. 8, right), indicating that EAPs coalesce during the formation of such structures. Quantification of clusters and particles/cluster in cell membrane areas expressing high or low content of ICAM-1 and VCAM-1 revealed an increase in cluster number in those areas containing higher numbers of adhesion molecules, whereas there was no significant change in the number of particles per cluster. EAPs therefore seem to be size restricted to nanometric dimensions (apparent mean size of ~300 nm; Fig. 7 A and Fig. S5 A, available at http://www.jcb.org/cgi/content/full/jcb.200805076/DC1).

Nearest neighbor analysis of the spatial pattern of immunogold-labeled ICAM-1 and VCAM-1 in the presence of CD9-LEL-GST showed that receptor spacing was increased compared with cells not treated or treated with heat-inactivated peptide (Fig. 7 B). CD9-LEL-GST also reduced the percentage of clustered receptors (Fig. 7 C) and partially disrupted their patterned distribution on the cell membrane (Fig. S5 B). CD9-LEL-GST thus seems to compete with endogenous CD9 for binding to itself homophilically and to other tetraspanins and partners, probably by blocking interactions and imposing steric hindrance, resulting in slower diffusion of EAP components and reduced receptor clustering, which in turn decreases adhesiveness.

Discussion

Plasma membranes contain different kinds of organized microdomains, all of which play important roles in sensing and processing information from the cell exterior. The composition and biophysical properties of lipid rafts, which are based on lipid–protein interactions, have been extensively studied (Kenworthy et al., 2004; Sharma et al., 2004). Much less is known about TEMs, which are primarily based on protein–protein interactions. Previous microscopy analysis of fixed samples and biochemical studies indicated that a network of specific protein–protein interactions may exist between tetraspanins and associated partners (Claas et al., 2001; Nydegger et al., 2006). In this study, we have used advanced analytical microscopy and single-molecule spectroscopy techniques to characterize the dynamic features and biophysical properties of TEMs in living primary human endothelial cells. Our results provide the first description of tetraspanin microdomains as physical entities in living cells with dynamic features that clearly differ from lipid rafts. The transiently transfected primary human endothelial cells used are a physiologically relevant cell model that expresses an appropriate repertoire of membrane tetraspanins and adhesion receptors. We show that these cells bear a particular kind of TEM enriched in membrane adhesion receptors to facilitate leukocyte–endothelial interactions that we have termed EAPs (Fig. 8, left). Moreover, we have characterized the molecular interactions of CD9 and CD151 tetraspanins and ICAM-1 and VCAM-1 adhesion receptors in EAPs, both at nude apical membrane and in the docking structures formed between endothelial cells and adhered leukocytes. Our results show that EAPs play an essential role in the spatial organization of the membrane and in the recruitment of ICAM-1 and VCAM-1 toward the contact area with adherent leukocytes, regulating endothelial cell adhesiveness (Fig. 8, right).

The coclustering of VCAM-1 at docking structures induced by ligand engagement of ICAM-1 and vice versa initially suggested that these adhesion receptors might interact with each other. However, the FRET–FLIM analysis only showed significant association for ICAM-1–ICAM-1, with negligible heterophilic interactions between ICAM-1 and VCAM-1. The existence of ICAM-1 homodimers has been shown before by biochemical approaches (Miller et al., 1995; Reilly et al., 1995). However, BIAcore affinity measurements revealed that a single ICAM-1 monomer, not dimeric ICAM-1, represents the complete, fully competent LFA-1–binding surface (Jun et al., 2001).

The possible role of tetraspanins in the corecruitment of these adhesion receptors was confirmed by additional FRET–FLIM analysis, which showed homophilic (CD9–CD9) and heterophilic (CD9–CD151) tetraspanin interactions as well as association of these tetraspanins with the adhesion receptors studied. Interestingly, the molecular interactions among tetraspanins and adhesion receptors show significant specificity, with a preferential association of CD9 with ICAM-1 and of CD151 with VCAM-1. Although full elucidation of the molecular complexity of EAPs requires additional studies, it is very likely that other tetraspanins and adhesion receptors are contained in these structures, interacting among themselves and with CD9, CD151, ICAM-1, and VCAM-1. Indeed, our data indicate that tetraspanin CD81 (Barreiro et al., 2005), CD44, PECAM-1/CD31, JAM-A, ICAM-2, and E-selectin (Fig. S4, B and C; and not depicted) all associate with tetraspanin CD9 and are included in EAPs. However, further studies are required to determine whether there are distinct kinds of EAPs with defined protein composition.

The diffusional behavior of EAP components was investigated by combining FRAP and FCS analyses; FRAP provided a qualitative overview of EAP diffusion at a microscopic level, and FCS allowed us to accurately quantify diffusion coefficients of EAP components at the single-molecule level. FRAP analyses indirectly examine the diffusion of an overall molecular population within a microscopic area at nude membrane or at sites of leukocyte anchorage. Therefore, a mixed steady-state molecular population (comprising proteins bound or unbound to cytoskeleton, coupled to partners, etc.) is considered for each measurement. From FRAP data collected at nude plasma membrane, we distinguished differences between the immobile fractions of VCAM-1 and ICAM-1. These data indicate important differences in the binding of these receptors to cortical cytoskeleton that deserve further analysis. In this regard, it has been described as a direct association of VCAM-1 with ezrin and moesin (Barreiro et al., 2002), whereas ICAM-1 interacts with α-actinin and colocalizes but does not directly associate with ezrin/radixin/moesin proteins in endothelial cells (Romero et al., 2002; Celli et al., 2006). The higher frequency of transiently immobilized

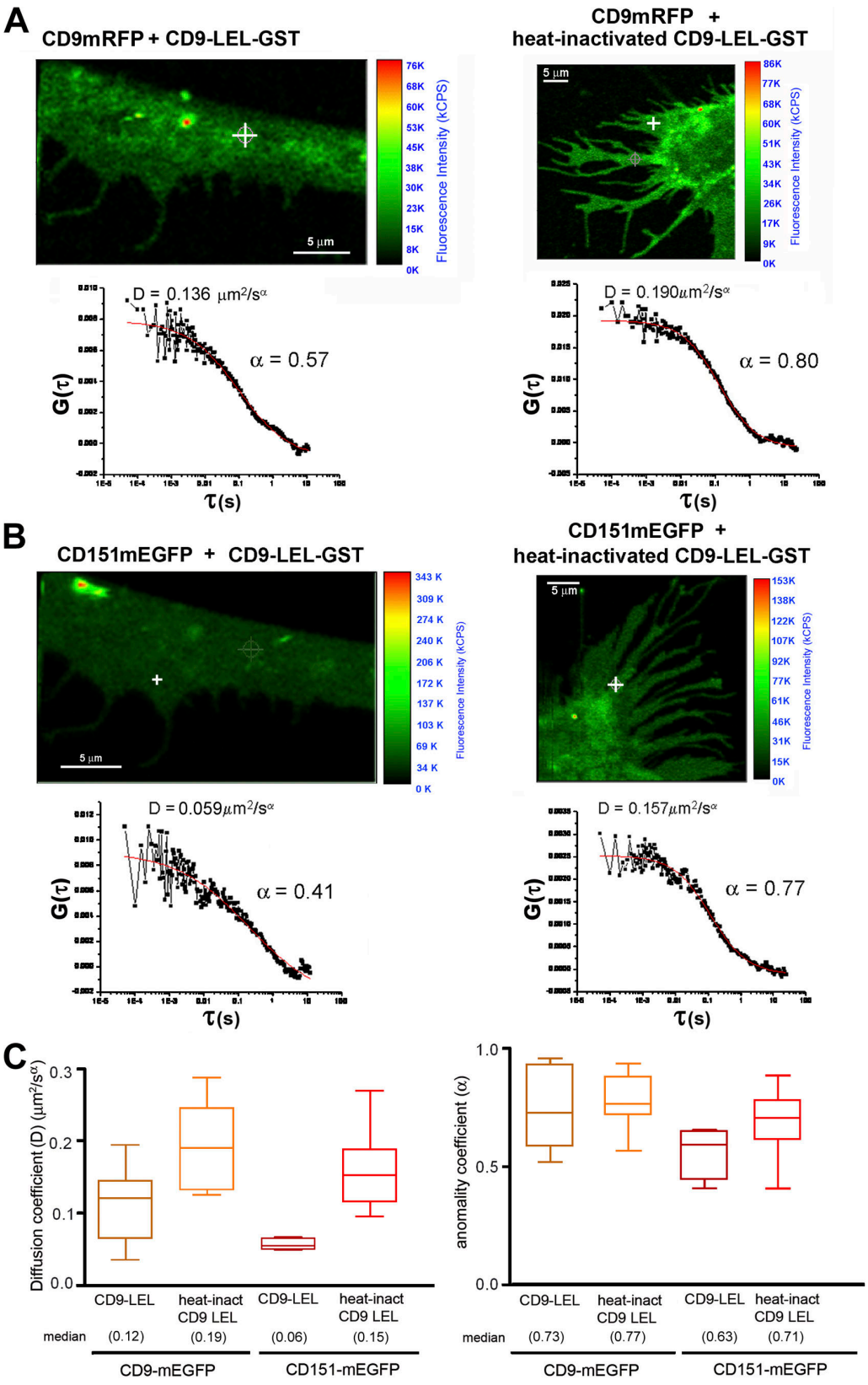

Figure 6. **CD9-LEL-GST perturbs EAP dynamics.** (A and B) Representative FCS measurements at the plasma membrane of endothelial cells transiently cotransfected with CD9-mRFP1 (A) and CD151-mEGFP (B) and treated with 250 μg/ml active or heat-inactivated CD9-LEL-GST. The figure shows the fluorescence intensity image, the ACF (black lines) derived from the fluorescence intensity trace acquired at the point marked with a white cross, the best-fitted curve using an anomalous diffusion model (red lines), and D and α coefficients. (C) Box-whisker plots show distributions of D and α values (as in Fig. 4). Statistical analysis and number of experiments are presented in Table S3 (available at http://www.jcb.org/cgi/content/full/jcb.200805076/DC1). kCPS, kilo counts per second.

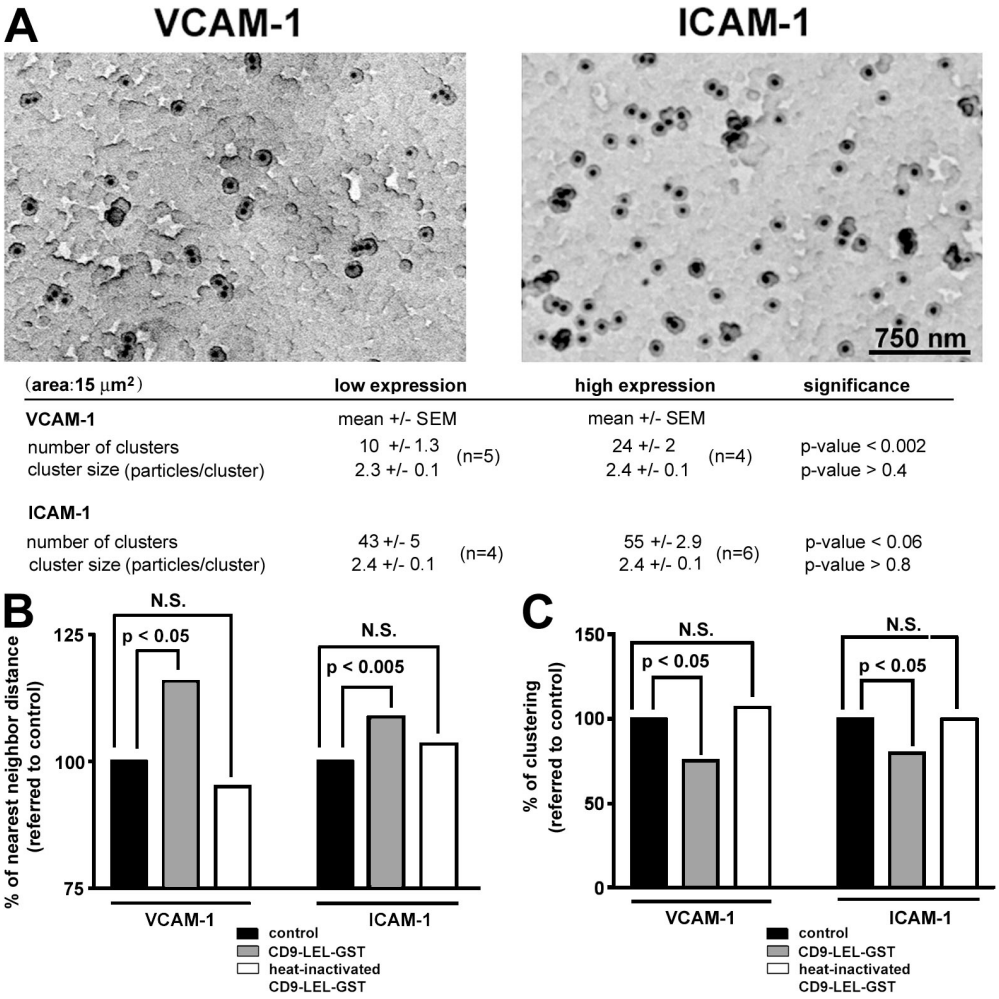

Figure 7. **Tetraspanins regulate endothelial adhesion receptor nanoclustering.** (A) TNF-α–activated endothelial cells were fixed and stained with anti–VCAM-1 or anti–ICAM-1 followed by 40-nm gold immunolabeling. Representative scanning electron microscope negative images of the endothelial plasma membrane are shown. Mean cluster number and size ± SEM for VCAM-1– and ICAM-1–containing microdomains analyzed in images with low or high particle number (i.e., indirect measurement of low or high receptor expression). Clustering parameters: δ = 100 and λ = 1 (see Materials and methods). (B) Gold particle coordinates from individual scanning electron microscope images (15-μm² plasma membrane) were used to compute nearest neighbor distances (see Materials and methods). Graphs show comparison of VCAM-1 or ICAM-1 nanoclustering based on nearest neighbor profiles from control, CD9-LEL-GST–, and heat-inactivated CD9-LEL-GST–treated samples with statistically comparable numbers of particles. The bar plot represents the mean of the Euclidean distance of the nearest neighbor for the total of *n* particles in the several images analyzed for each treatment. (C) Clustering rates were computed from the samples in B (see Materials and methods). Clustering parameters: VCAM-1, δ = 205 and λ = 2; and ICAM-1, δ = 140 and λ = 2. Statistical significance in the figure was based on a Student's *t* test.

molecules in the case of VCAM-1 might produce a decrease in the average apparent D coefficient for this molecular species because FRAP calculations are made on an overall molecular population. In fact, these apparent D coefficients fitted by a simple diffusion model do not reveal the real diffusional behavior of the receptors, which turned out to be undistinguishable when precisely measured by single-molecule FCS analysis fitted by an anomalous diffusion model. Diffusional analyses by FCS thus complement the FRAP data.

When we used FRAP to analyze the diffusion of GPI-EGFP, a lipid raft marker widely used in microscopy studies (Varma and Mayor, 1998; Kenworthy et al., 2004), we found that this protein diffused much faster than tetraspanins and other EAP components and showed almost full fluorescence recovery. In addition, most D coefficients for EAP proteins that we have obtained using FCS are much lower than those reported for prototypic lipid raft proteins (Lenne et al., 2006). Moreover, GPI-EGFP was unaffected by engagement of integrin-bearing leukocytes, whereas EAP dynamics were altered. In fact, the delay observed for nonligand-engaged EAP components at docking structures could well be the result of their transient interaction with ligand-immobilized ICAM-1 or VCAM-1. These immobile complexes at docking sites could thus act as physical constraints on the mobility of the overall molecular populations analyzed, producing a net restriction in local diffusion. The fact that each adhesion receptor is less affected than tetraspanins by ligand engagement of the other receptor supports a model of tetraspanin-dependent receptor coclustering. The higher relative frequency of fast diffusion by tetraspanins indicates that they are more dynamically exchanged between EAPs than are adhesion receptors, further supporting their role as the active organizers of these microdomains. Moreover, adhesion receptors

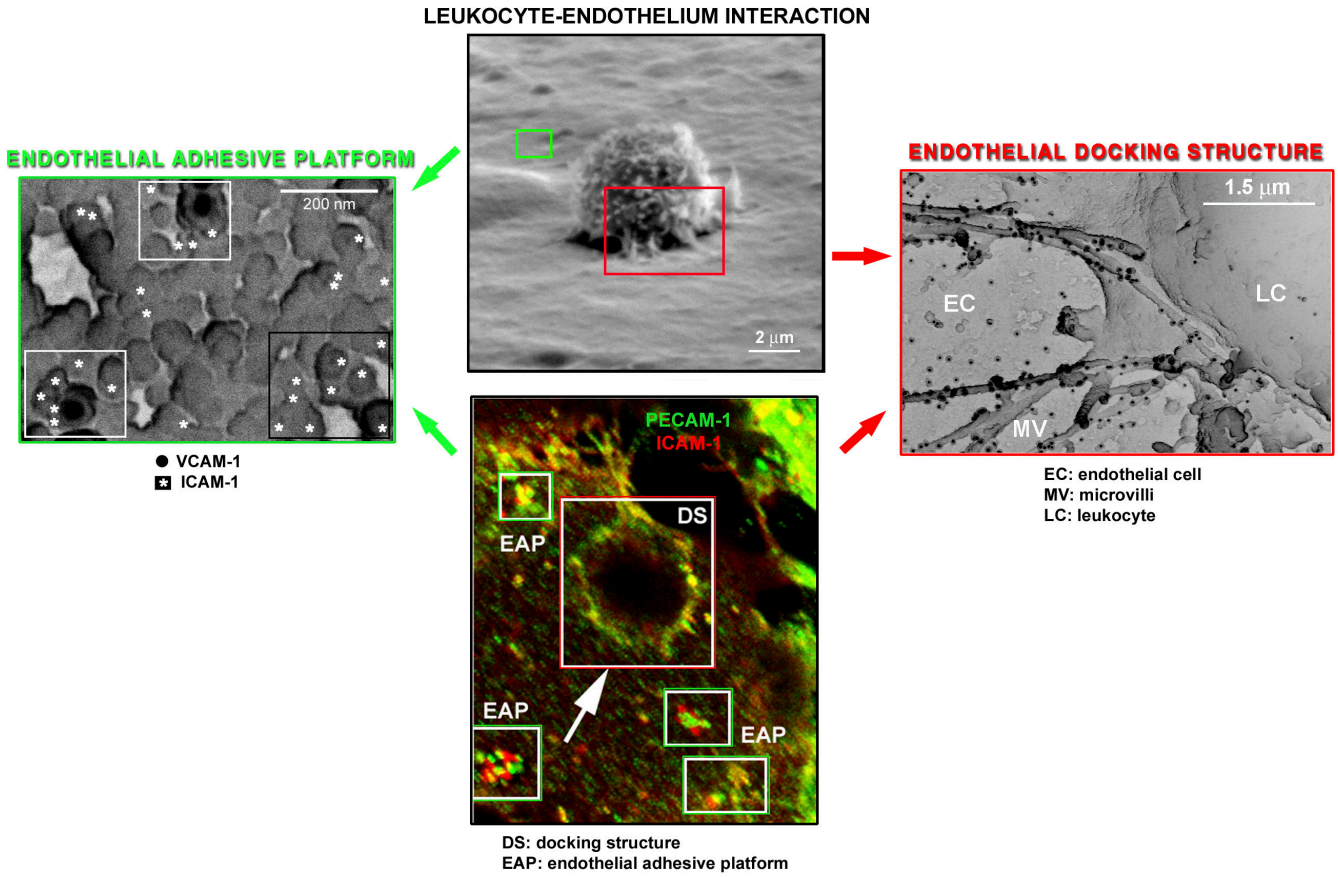

Figure 8. **Scheme of tetraspanin-enriched EAPs and docking structures.** (top middle) Scanning electron microscopy image of a peripheral blood lymphocyte interacting with the apical membrane of an endothelial cell under flow conditions. The green square marks a zone of nude membrane containing EAPs as shown at high magnification in the left panel. The red square highlights the endothelial docking structure, as shown at a nanometric scale in the right panel. EAPs are preformed nanoclusters that serve as nucleating units for integrin ligands and their tetraspanin partners, whereas docking structures are microscopic clusters of EAPs organized in microvilli around adherent leukocytes. (bottom middle) Immunofluorescence staining showing the macroscopic appearance of EAPs and docking structures. K562 LFA-1 was adhered (30 min) to TNF-α–activated HUVECs. Samples were fixed and double stained with anti–PECAM-1 and biotin-conjugated anti–ICAM-1. Confocal stacks were obtained, and an orthogonal maximal projection is displayed. Microscopic-sized clusters of EAPs in this image. (left) Activated endothelial cells were fixed and double stained with 40 nm VCAM-1 and 15-nm ICAM-1 gold particles. The panel shows a representative negative scanning electron microscopy image from the nude apical endothelial plasma membrane. The white asterisks mark the 15-nm anti–ICAM-1 gold particles, and the black dots are the 40-nm anti–VCAM-1 gold particles. The white boxes depict regions of VCAM-1–ICAM-1 heteroclustering, whereas the black box shows an ICAM-1 homoclustering zone. (right) T lymphoblasts were adhered to activated endothelial cells (5 min). Fixed cells were stained with anti–ICAM-1 and 40-nm immunolabeled gold. A representative negative scanning electron microscopy image shows the preferential localization of gold particles at the microvilli of the endothelial docking structure formed around a lymphoblast, where EAPs coalesce.

exhibit a higher anomality in diffusion, which accounts for their preferential binding to cortical cytoskeleton and transient immobilization compared with tetraspanins (Sala-Valdes et al., 2006). However, further studies are needed to define the residence time of molecules within EAPs. The mix of endogenous and exogenous protein populations precludes precise determination of the stoichiometry of submicrometer-sized EAPs. Nonetheless, analysis of brightness from the photon-counting histograms obtained during FCS measurements revealed the existence of complexes containing more than one fluorescently labeled molecule. This was also confirmed by fluorescence cross-correlation spectroscopy analysis (unpublished data).

FRET analysis confirmed a degree of specificity inside the preexistent EAPs before leukocyte binding. The preferential interactions of ICAM-1 with CD9 and VCAM-1 with CD151 are evident in the FRETeff for these pairs. FRET–FLIM analysis shows that interactions between tetraspanins and tetraspanin adhesion receptors are more frequent compared with ICAM-1–ICAM-1 interactions, which supports the central role of tetraspanins in the molecular dynamics of adhesion receptors, strengthening the concept of EAPs as the basic organizational unit of endothelial adhesion receptors on the apical plasma membrane.

The regulation of endothelial adhesion receptor avidity by their inclusion in tetraspanin-enriched EAPs represents a conceptual advance in the understanding of leukocyte–endothelium interactions. Leukocyte integrin activity can be regulated by conformational changes (affinity) and/or clustering at the plasma membrane (avidity; Luo et al., 2007). In contrast, no regulatory mechanism apart from transcription has been described before for endothelial integrin ligands (Collins et al., 1995). Our data demonstrate that tetraspanin and adhesion receptor colocalization does indeed reflect highly specific and organized interactions among them, forming specialized TEMs (EAPs; Fig. 8, left and middle panels illustrate preformed EAPs). Inclusion of ICAM-1 and VCAM-1 in EAPs allows homo- and heteroclustering of

both molecules at the contact area with the adhered leukocyte independent of ligand binding and actin cytoskeleton anchorage (Fig. 8, right and middle panels illustrate a docking structure around the adhered leukocyte). This novel role of tetraspanins seems to represent a supramolecular level of regulation not previously envisaged for integrin ligands. Additional tetraspanin molecules could be involved in regulating the molecular dynamics and organization of EAPs, among them CD81, which is also localized at endothelial docking structures (Barreiro et al., 2005) and which, in leukocytes, is able to act as a homeostatic avidity facilitator of VLA-4 (Feigelson et al., 2003).

The important role of tetraspanins in the molecular dynamics of EAPs is also supported by our results with the CD9-LEL-GST–blocking peptide. It seems evident that this CD9-blocking peptide perturbs EAP dynamics by competing with endogenous CD9 for binding to partners and other tetraspanins. As CD9 is the most abundant of the analyzed EAP components, intercalation of CD9-blocking peptides into EAPs would alter the patterned distribution and mobility of all the proteins embedded within them, providing an explanation for the decrease in receptor-binding strength. EAPs thus appear to endow ICAM-1 and VCAM-1 with the proper spatial distribution to exert their adhesive functions, promoting their clustering and, therefore, enhancing their avidity for their ligands expressed on leukocytes. Supramolecular organization at the nanoscale has been reported for other receptor molecules, including LFA-1 integrin on leukocytes and the C-lectin receptor dendritic cell–specific ICAM-grabbing nonintegrin on dendritic cells (Cairo et al., 2006; Cambi et al., 2006; de Bakker et al., 2007). Whether these molecules are included within TEMs on the leukocyte plasma membrane is an interesting issue that deserves investigation.

With the reagents currently available, it is not possible to address whether endothelial receptors undergo conformational change because of their interaction with tetraspanins. However, it will be of interest to identify the critical amino acid sequences in tetraspanins and adhesion receptors that participate in their lateral interactions. This information would have potential use in the future design of therapeutic blocking agents directed at reducing the adhesiveness of endothelial cells toward circulating leukocytes. Such agents might provide novel therapeutic strategies for the treatment of chronic inflammatory and autoimmune diseases in a more general manner than existing therapies focused on the inhibition of a particular adhesion pathway mediated by a single integrin ligand.

In summary, our data indicate that EAPs are specialized tetraspanin-based membrane microdomains that regulate the avidity of several adhesion receptors integrated in them, acting as a mechanism to organize molecules with similar characteristics and functions and thereby facilitating their coordinated action in rapidly occurring processes such as extravasation.

Materials and methods

Cells

HUVECs were cultured as described previously (Barreiro et al., 2002). K562 erythroleukemic cells, which endogenously express β1 integrin, were stably transfected with integrin α4 to yield cells expressing α4β1 integrin/VLA-4 or with integrin αLβ2/LFA1. K562 clones and T lymphoblasts were cultured as described previously (Barreiro et al., 2002). Integrin inhibitors BIO5192 and BIRT377 were provided by Biogen Idec and Boehringer Ingelheim, respectively.

Antibodies

Anti-CD151 (LIA1/1), anti–VE-cadherin (TEA1/31), and anti-CD9 (VJ1/20) mAbs have been described previously (Yanez-Mo et al., 1998). P8B1 (anti–VCAM-1), MEM-111 and Hu5/3 (anti–ICAM-1), and 8C3 (anti-CD151) mAbs were provided by E.A. Wayner (Fred Hutchinson Cancer Research Center, Seattle, WA), V. Horejsi (Academy of Sciences of the Czech Republic, Prague, Czech Republic), F.W. Luscinskas (Brigham and Women's Hospital, Harvard Medical School, Boston, MA), and K. Sekiguchi (Osaka University, Osaka, Japan), respectively. Anticaveolin antibody was purchased from Sigma-Aldrich.

Recombinant DNA constructs and proteins and transfections

EGFP-tagged ICAM-1, VCAM-1, CD9, and CD151 have been previously described (Barreiro et al., 2002, 2005; Garcia-Lopez et al., 2005). The construct encoding VCAMΔCyt, a C-terminally truncated VCAM-1 protein in which the first cytoplasmic charged residue is retained to ensure proper membrane insertion, was generated by PCR using the human VCAM-1 cDNA as template and CTCGAGTCTCATCACGACAGCAAC and CTATCTTGCAAAGTAAATTATC as 5′ and 3′ primers, respectively. The PCR product containing a stop codon at position 1722 was cloned into pcDNA3.1/V5-His-TOPO (Invitrogen), and correct expression of VCAMΔCyt at the plasma membrane was tested. The equivalent ICAM-1–tailless construct, but fused to EGFP, was provided by F.W. Luscinskas. For FCS and FRET–FLIM experiments, monomeric green and red variants of ICAM-1, VCAM-1, CD9, and CD151 were generated. mEGFP constructs were obtained by A206K point mutation (Zacharias et al., 2002; Zhang et al., 2002) using the Quick Mutagenesis kit (Stratagene). The mRFP1 variants were generated by subcloning the corresponding EGFP constructs into an mRFP1 vector provided by R.Y. Tsien (University of California, San Diego, La Jolla, CA; Campbell et al., 2002). The GPI-EGFP construct was provided by M.A. del Pozo (Centro Nacional de Investigaciones Cardiovasculares, Madrid, Spain). The LEL of GST-fused human CD9 wild type was obtained as described previously (Barreiro et al., 2005).

HUVECs were transiently transfected by electroporation (Barreiro et al., 2005) or with lipofectin (Invitrogen) according to the manufacturer's protocol. Transfected cells were grown to confluence for 24–48 h on 20 µg/ml fibronectin (FN; Sigma-Aldrich)-precoated glass coverslips or glass-bottomed dishes (WillCo Wells). Activation with 20 ng/ml TNF-α was performed for 20 h unless indicated otherwise.

Cell adhesion, immunofluorescence, and confocal microscopy

Confluent HUVECs on FN-coated coverslips were activated with TNF-α. Then, K562 clones or T lymphoblasts were added. Adhesion of K562 LFA-1 to activated HUVEC monolayers was assayed in the presence of 1 mM Mn^{2+} to activate integrins. Where indicated, T lymphoblasts were treated with 10 µg/ml BIO5192 or 10 µM BIRT377 for 5 min before adhesion assay. After incubation, samples were washed and fixed in 4% paraformaldehyde and processed for immunofluorescence (Yanez-Mo et al., 1998). A series of optical sections were obtained at 21°C with a confocal laser-scanning unit (TCS-SP5; Leica) coupled to a microscope (DMI6000; Leica) using an HCX PL APO CS 63× NA 1.3 glycerol immersion objective. Images were analyzed with confocal software (Leica).

Bead adhesion

TNF-α–activated HUVECs were incubated for 30 min with Dynabeads coated with antitetraspanin, anti–VCAM-1, or anti–VE-cadherin mAb (Invitrogen) and were fixed and stained with biotinylated anti–ICAM-1 mAb.

Sucrose density gradient fractionation

Confluent TNF-α–activated HUVECs were rinsed with PBS and lysed for 20 min in 250 µl of 25 mM Tris-HCl, pH 7.5, 150 mM NaCl, and 1% Brij96 at 4°C. The cell lysate was homogenized by passing the sample through a 22-gauge needle. The extract was brought to 40% sucrose (wt/wt) in a final volume of 4 ml and placed at the bottom of an 8-ml 5–30% linear sucrose gradient. Gradients were ultracentrifuged to equilibrium for 20 h at 39,000 rpm at 4°C in a rotor (SW41; Beckman Coulter). 1-ml fractions were harvested from the bottom of the tube. Aliquots from each fraction were subjected to SDS-PAGE and Western blotting with appropriate antibodies.

FRAP

Cells transfected with EGFP fusion proteins (VCAM-1–, ICAM-1–, CD9-, CD151-, ICAM-1ΔCyt–, and GPI-EGFP) were plated on FN-coated coverslips.

After 24 h, cells were stimulated with TNF-α, and FRAP experiments were performed within 48 h of plating. To analyze FRAP at the endothelial docking structure, an adhesion assay was conducted using K562 α4 or LFA-1. Live cell microscopy was performed with a confocal laser-scanning unit (TCS-SP2; Leica) coupled to a microscope (DMIRBE; Leica) using the 488-nm Ar laser line and an HCX PL APO lambda blue 63× NA 1.4 oil immersion objective. During observation, plates were maintained at 37°C in a 5% CO_2 atmosphere using an incubation system (LaCon GbR/PeCon GmbH). Laser power for bleaching was maximal but was reduced to 10% for imaging. 10 single-section prebleach images were acquired followed by three iterative bleach pulses of 1.7 s each. 10 single-section images were then collected at 1.7-s intervals followed by 20 images every 10 s and finally 15 images every 30 s for a total experimental time of ∼650 s.

Fluorescence recovery in the bleached region was measured as average signal intensity. All recovery curves were generated from background-subtracted and bleaching-corrected images. Moreover, the fluorescence signal was normalized to the prebleach signal in the same region of interest.

The mobile fraction (R) corresponds to the final value of the recovered fluorescence intensity, and the immobile fraction is obtained as 1 − R. The half-time of recovery is the time from bleaching to the time when the fluorescence intensity is half of the final recovered intensity. All three variables were directly obtained from the normalized mean fluorescence recovery curves.

The averaged recoveries were fitted with the equation

$$F(t) = \frac{F_0 + (R \times (F^0 - F_0) + F_0) \times (t/t_{1/2})}{1 + (t/t_{1/2})},$$

where F_0 = fluorescence intensity at the first time point after bleach, F^0 = fluorescence intensity before bleach, R = mobile fraction, and $t_{1/2}$ = half recovery time. Apparent diffusion coefficients from averaged recovery half-times were derived using a simple Brownian diffusion model. Averaged immobile fractions (1 − R) were derived from averaged fitted curves.

The possible perturbation of membrane dynamics that might result from differential exogenous expression of tagged proteins was overcome in FRAP experiments by making a large number of measurements in several batches of transiently transfected primary endothelial cells and exhaustive statistical analysis. To assess the statistical significance of differences between FRAP recovery curves, we derived a *t* test analysis on the average fitted curves for each protein in each condition.

Hetero-FRET by donor FLIM in intact living cells

HUVECs were single transfected with mEGFP standards or cotransfected with mEGFP–mRFP1 pairs and seeded on FN-coated glass-bottomed dishes. After 24 h and without TNF-α treatment, the culture medium was replaced with a phenol red–free medium for optimal image acquisition. FLIM was performed using the digital frequency domain method and the new FLIM box, recently described in detail (Colyer et al., 2008), which were implemented at the Laboratory of Fluorescence Dynamics (University of California, Irvine, Irvine, CA) on a commercial confocal system (FluoView 1000; Olympus). Excitation was provided by a modulated 471-nm diode laser (ISS, Inc.). A 40× 1.2 NA water immersion objective (Carl Zeiss, Inc.) was used. Data were acquired and processed by SimFCS software (developed at the Laboratory of Fluorescence Dynamics). The scan area (256 × 256 pixels) corresponds to 32 × 32 μm^2. Before cell measurements, concentrated fluorescein at pH 9.0 was measured. Fluorescein lifetime (4.04 ns) was determined separately in a fluorometer (PC1; ISS, Inc.).

The FLIM analysis for deriving FRETeff was performed using the phasor FLIM method recently described (Caiolfa et al., 2007; Digman et al., 2008) and commented on (Wouters and Esposito, 2008). The contour plots associated with each image show the entire distribution of the donor fluorescence lifetimes in the image. The distribution was obtained by converting the multiexponential fluorescence decays acquired in each pixel into the graphical representation of a phasor. In brief, the phasor transformation does not assume any fitting model for fluorescence lifetime decays. It simply expresses the overall decay in each pixel in terms of a point of (s, g) polar coordinates in the so-called "universal circle" (Redford and Clegg, 2005). In each plot, the green line represents the position of all phasors having 0% FRETeff and variable cellular autofluorescence. These points were derived from the lifetime analysis in cells expressing only the donor molecules, whereas untransfected cells were used as a control for autofluorescence. Once the phasors of the unquenched donors and of the cell autofluorescence (green line in the phasor plots) are known, the FRET trajectory in the phasor plot can be calculated according to the classical relationship FRETeff = $[1 - (\tau_{donor-acceptor})/\tau_{donor}]$ and define the mean phasors of mEGFP constructs quenched by 50% FRET in the presence of the acceptor and with different contributions from cell autofluorescence (red line in all phasor plots). In all of our experiments, phasors resulting from any combination of unquenched donors, FRET-quenched donors, and cell autofluorescence have been found within the area delimited by the green and red lines in the phasor plots. The localization and distribution of the phasors of mEGFP constructs were not affected by the kind of protein linked to the fluorophore or by the cells in which they were expressed. Endogenous untagged proteins expressed in our cell model may interfere with FRET. To minimize interaction between endogenously and exogenously expressed tagged proteins in FLIM analyses, quantifications were performed in resting endothelial cells, where tetraspanin expression is unaltered, ICAM-1 levels are low, and VCAM-1 plasma membrane expression is negligible. Given that endogenous CD151 and CD9 expression is much higher than ICAM-1 in resting endothelial cells, FRETeff from measurements involving tetraspanin proteins may be underestimated. Moreover, because CD9, CD151, and ICAM-1 can homodimerize, the association of two green or red molecular species makes hetero-FRET events even more improbable. To substantiate the experimental data on the absence of ICAM-1–VCAM-1 heterodimers, ICAM-1 or VCAM-1 was used indistinctly as a donor in FRET–FLIM experiments.

FCS

HUVECs were transiently single or double transfected as for FLIM and treated either with growth factors (resting conditions) or with 20 ng/ml TNF-α (activated conditions). Intensity fluctuations were recorded on the described setup (Caiolfa et al., 2007) based on a dual-channel confocal fluorescence correlation spectrometer (ALBA; ISS, Inc.) equipped with avalanche photodiodes (SPCM-AQR-15; PerkinElmer) and interfaced to an inverted microscope (TE300; Nikon). A 60× 1.2 NA plan Apo water immersion objective was used. Excitation was provided at 488 nm by a tunable Ar ion laser (Melles Griot) and at 594 nm by a HeNe laser (Melles Griot). Calibration and data collection were performed according to the procedures previously described (Caiolfa et al., 2007).

The ACFs were best fitted using the anomalous diffusion model (Banks and Fradin, 2005), according to the equation

$$G(\tau) = \frac{1}{N} \times \frac{1}{1 + \left(\frac{\tau}{\tau_D}\right)^{\alpha}},$$

where N is the average number of molecules in the excitation volume, τ is the increment of time, τ_D is the diffusion time, and α is the anomality coefficient. Accordingly, the diffusion coefficient (D) is derived from the relationship $D = \omega^2/4\tau^{\alpha}$.

In FCS experiments, endogenous proteins were in excess compared with corresponding fluorescent-tagged variants, minimizing artifacts as a result of differences in local concentrations of the latter. FCS experiments were performed both either in resting or in TNF-α–activated HUVECs, not finding statistically significant differences in diffusion between the treatments.

Scanning electron microscopy

Endothelial monolayers were activated with TNF-α in the absence or presence of 250 µg/ml of active or heat-inactivated (5 min at 90°C) CD9-LEL-GST peptide. T lymphoblasts were added when indicated. Cells were fixed in 2% paraformaldehyde/PBS and immunolabeled with P8B1 (anti–VCAM-1), Hu5/3 (anti–ICAM-1), or biotinylated MEM-111 (anti–ICAM-1) as primary antibodies and 40 nm of gold-coupled anti–mouse antibody or 15 nm of gold-coupled streptavidin (British Biocell International) as detection reagents. Samples were fixed in 2.5% glutaraldehyde/PBS, sequentially dehydrated, critical point dried, and covered with a 5-nm carbon layer. Images were obtained with a scanning electron microscope (S-4100; Hitachi) at an acceleration voltage of 12 kV and a 4-mm working distance. Images were processed with Metamorph software (MDS Analytical Technologies).

Nearest neighbor distances and k nearest neighbor (knn) profiles

For each image, we computed the knn distance vector that contains in its i^{th} position the mean of the distances between objects and their i^{th} nearest neighbor. Comparison of knn profiles allows us to establish similarities and discrepancies between different treatments in terms of aggregation and dispersion of the clouds of points in the image. The knn distances were assumed to be independent realizations of a normal distribution (the null hypothesis of normality could not be rejected using a Shapiro-Wilk test). Because the knn profile might be dependent on the number of objects, the analysis was performed

using images that contained a similar number of objects. Nearest neighbor analysis was evaluated by using a custom-written software based on R language (R Development Core Team [2006]. R: a language and environment for statistical computing. R Foundation for Statistical Computing, Vienna, Austria. ISBN 3-900051-07-0. http://www.R-project.org).

Cluster and statistical significance

The dissimilarities between clustered point patterns for different images were established in terms of the proportion of aggregation, defined for a given image, I_v, as the proportion of gold particles, p_v, that are included in any cluster identified in I_v. To identify the cluster pattern of I_v, a cluster agglomerative algorithm based on Euclidean distances between points was developed and implemented in R language. In the way that the clusters are defined, the minimum size of the cluster is $\lambda + 1$. The algorithm allows the formation of clusters of any shape, retaining points that are close enough to each other to be considered as aggregated. This minimum distance at aggregation is set by the parameter δ. The criteria to select different values for δ and λ parameters were based on the differential number of particles in the images used for the various analyses. For every image, I_v, and corresponding δ and λ, a point cluster pattern is identified, and the proportion of points, p_v, that are included in any cluster is computed. Then, the differences between families of images can be established in terms of the different proportions, p_v. The statistical significance among families of images was assessed with a Student's *t* test using the asin transformation of p_v as $\arcsin(\sqrt{p_v})$.

Spatial randomness

To statistically assess whether the points in a given image are located in random positions, we followed the method for testing spatial randomness previously described (Manly, 1997). We computed the knn vector for each observed image. The null hypothesis knn vector was generated by simulating 100 sets of images with points located at random positions, considering that all points have the same probability of being situated anywhere in the image and are independent of each other. Random distribution of points is expected to produce greater knn values, so the significance level was defined for every i^{th} knn distance as the proportion of values in the null distribution that were greater than or equal to the observed value. Spatial randomness analysis was evaluated by using a custom-written software based on R language.

Statistical analysis

All statistical analyses (one-sided or two-sided *t* tests and analysis of variance with Tukey's Honest Significant Difference) were performed with R language or Prism software (GraphPad Software, Inc.).

Online supplemental material

Fig. S1 shows controls for FRET–FLIM experiments and study of the specificity of molecular interactions within the EAPs. Fig. S2 shows involvement of tetraspanin microdomains in the corecruitment of endothelial adhesion receptors. Fig. S3 shows a comparison of dynamic behaviors of EAP constituents and cytoplasmic tail–truncated ICAM-1 mutant at nude plasma membrane and at docking structures. Fig. S4 shows the relative frequency histograms for D and α coefficients obtained by FCS and study of other adhesion receptors included in EAP. Fig. S5 shows examples of receptor clustering patterns and spatial randomness analysis. Table S1 shows the derived apparent D coefficients from Fig. 3 A. Table S2 shows the statistical analysis on fluorescence recovery curves from Fig. 3 and Fig. S3. Table S3 shows the statistical analysis on the diffusion coefficients from Figs. 4 and 6. Online supplemental material is available at http://www.jcb.org/cgi/content/full/jcb.200805076/DC1.

We thank N. Cortadellas, R. Fontarnau, E. Prats, A. Domínguez (Serveis Científicotècnics de la Universitat de Barcelona), M. Sala-Valdés, A. Batista, D. Megías, R. Samaniego (Hospital Gregorio Marañón), G. Malengo, R. Colyer, C. Lee, and T.L. Hazlett for technical assistance and S. Barlett for critical reading of the manuscript.

This work was funded by Salud grant SAF2008-02635, Biología Fundamental grant 2005-08435/Biología Molecular y Celular, Ayuda a la Investigación Básica 2002 Fundación Juan March, and the Lilly Foundation (to F. Sanchez-Madrid), National Institutes of Health grant P41-RRO3155 (to E. Gratton), European Union grant LSHG-CT-2003-502935 (to O. Barreiro), and Red Temática de Investigación Cooperativa en Enfermedades Cardiovasculares grant RD06/0014-0030. The Centro Nacional de Investigaciones Cardiovasculares (CNIC) is supported by the Spanish Ministry of Health and Consumer Affairs and the Pro-CNIC Foundation.

Submitted: 14 May 2008
Accepted: 9 September 2008

References

Anderson, R.G., and K. Jacobson. 2002. A role for lipid shells in targeting proteins to caveolae, rafts, and other lipid domains. *Science.* 296:1821–1825.

Banks, D.S., and C. Fradin. 2005. Anomalous diffusion of proteins due to molecular crowding. *Biophys. J.* 89:2960–2971.

Barreiro, O., M. Yanez-Mo, J.M. Serrador, M.C. Montoya, M. Vicente-Manzanares, R. Tejedor, H. Furthmayr, and F. Sanchez-Madrid. 2002. Dynamic interaction of VCAM-1 and ICAM-1 with moesin and ezrin in a novel endothelial docking structure for adherent leukocytes. *J. Cell Biol.* 157:1233–1245.

Barreiro, O., M. Yanez-Mo, M. Sala-Valdes, M.D. Gutierrez-Lopez, S. Ovalle, A. Higginbottom, P.N. Monk, C. Cabanas, and F. Sanchez-Madrid. 2005. Endothelial tetraspanin microdomains regulate leukocyte firm adhesion during extravasation. *Blood.* 105:2852–2861.

Berditchevski, F. 2001. Complexes of tetraspanins with integrins: more than meets the eye. *J. Cell Sci.* 114:4143–4151.

Berditchevski, F., and E. Odintsova. 2007. Tetraspanins as regulators of protein trafficking. *Traffic.* 8:89–96.

Caiolfa, V.R., M. Zamai, G. Malengo, A. Andolfo, C.D. Madsen, J. Sutin, M. Digman, E. Gratton, F. Blasi, and N. Sidenius. 2007. Monomer-dimer dynamics and distribution of GPI-anchored uPAR are determined by cell surface protein assemblies. *J. Cell Biol.* 179:1067–1082.

Cairo, C.W., R. Mirchev, and D.E. Golan. 2006. Cytoskeletal regulation couples LFA-1 conformational changes to receptor lateral mobility and clustering. *Immunity.* 25:297–308.

Cambi, A., B. Joosten, M. Koopman, F. de Lange, I. Beeren, R. Torensma, J.A. Fransen, M. Garcia-Parajo, F.N. van Leeuwen, and C.G. Figdor. 2006. Organization of the integrin LFA-1 in nanoclusters regulates its activity. *Mol. Biol. Cell.* 17:4270–4281.

Campbell, R.E., O. Tour, A.E. Palmer, P.A. Steinbach, G.S. Baird, D.A. Zacharias, and R.Y. Tsien. 2002. A monomeric red fluorescent protein. *Proc. Natl. Acad. Sci. USA.* 99:7877–7882.

Carman, C.V., and T.A. Springer. 2003. Integrin avidity regulation: are changes in affinity and conformation underemphasized? *Curr. Opin. Cell Biol.* 15:547–556.

Celli, L., J.J. Ryckewaert, E. Delachanal, and A. Duperray. 2006. Evidence of a functional role for interaction between ICAM-1 and nonmuscle alpha-actinins in leukocyte diapedesis. *J. Immunol.* 177:4113–4121.

Claas, C., C.S. Stipp, and M.E. Hemler. 2001. Evaluation of prototype transmembrane 4 superfamily protein complexes and their relation to lipid rafts. *J. Biol. Chem.* 276:7974–7984.

Colyer, R.A., C. Lee, and E. Gratton. 2008. A novel fluorescence lifetime imaging system that optimizes photon efficiency. *Microsc. Res. Tech.* 71:201–213.

Collins, T., M.A. Read, A.S. Neish, M.Z. Whitley, D. Thanos, and T. Maniatis. 1995. Transcriptional regulation of endothelial cell adhesion molecules: NF-kappa B and cytokine-inducible enhancers. *FASEB J.* 9:899–909.

Charrin, S., S. Manie, C. Thiele, M. Billard, D. Gerlier, C. Boucheix, and E. Rubinstein. 2003. A physical and functional link between cholesterol and tetraspanins. *Eur. J. Immunol.* 33:2479–2489.

Chattopadhyay, N., Z. Wang, L.K. Ashman, S.M. Brady-Kalnay, and J.A. Kreidberg. 2003. $\alpha 3\beta 1$ integrin-CD151, a component of the cadherin-catenin complex, regulates PTPmu expression and cell-cell adhesion. *J. Cell Biol.* 163:1351–1362.

Cherukuri, A., T. Shoham, H.W. Sohn, S. Levy, S. Brooks, R. Carter, and S.K. Pierce. 2004. The tetraspanin CD81 is necessary for partitioning of coligated CD19/CD21-B cell antigen receptor complexes into signaling-active lipid rafts. *J. Immunol.* 172:370–380.

de Bakker, B.I., F. de Lange, A. Cambi, J.P. Korterik, E.M. van Dijk, N.F. van Hulst, C.G. Figdor, and M.F. Garcia-Parajo. 2007. Nanoscale organization of the pathogen receptor DC-SIGN mapped by single-molecule high-resolution fluorescence microscopy. *Chemphyschem.* 8:1473–1480.

Digman, M.A., V.R. Caiolfa, M. Zamai, and E. Gratton. 2008. The Phasor approach to fluorescence lifetime imaging analysis. *Biophys. J.* 94:2320–2332.

Feigelson, S.W., V. Grabovsky, R. Shamri, S. Levy, and R. Alon. 2003. The CD81 tetraspanin facilitates instantaneous leukocyte VLA-4 adhesion strengthening to vascular cell adhesion molecule 1 (VCAM-1) under shear flow. *J. Biol. Chem.* 278:51203–51212.

Garcia-Lopez, M.A., O. Barreiro, A. Garcia-Diez, F. Sanchez-Madrid, and P.F. Penas. 2005. Role of tetraspanins CD9 and CD151 in primary melanocyte motility. *J. Invest. Dermatol.* 125:1001–1009.

Gordon-Alonso, M., M. Yanez-Mo, O. Barreiro, S. Alvarez, M.A. Munoz-Fernandez, A. Valenzuela-Fernandez, and F. Sanchez-Madrid. 2006. Tetraspanins CD9 and CD81 modulate HIV-1-induced membrane fusion. *J. Immunol.* 177:5129–5137.

Hemler, M.E. 2003. Tetraspanin proteins mediate cellular penetration, invasion, and fusion events and define a novel type of membrane microdomain. *Annu. Rev. Cell Dev. Biol.* 19:397–422.

Hemler, M.E. 2005. Tetraspanin functions and associated microdomains. *Nat. Rev. Mol. Cell Biol.* 6:801–811.

Ho, S.H., F. Martin, A. Higginbottom, L.J. Partridge, V. Parthasarathy, G.W. Moseley, P. Lopez, C. Cheng-Mayer, and P.N. Monk. 2006. Recombinant extracellular domains of tetraspanin proteins are potent inhibitors of the infection of macrophages by human immunodeficiency virus type 1. *J. Virol.* 80:6487–6496.

Jun, C.D., M. Shimaoka, C.V. Carman, J. Takagi, and T.A. Springer. 2001. Dimerization and the effectiveness of ICAM-1 in mediating LFA-1–dependent adhesion. *Proc. Natl. Acad. Sci. USA.* 98:6830–6835.

Kenworthy, A.K., B.J. Nichols, C.L. Remmert, G.M. Hendrix, M. Kumar, J. Zimmerberg, and J. Lippincott-Schwartz. 2004. Dynamics of putative raft-associated proteins at the cell surface. *J. Cell Biol.* 165:735–746.

Kropshofer, H., S. Spindeldreher, T.A. Rohn, N. Platania, C. Grygar, N. Daniel, A. Wolpl, H. Langen, V. Horejsi, and A.B. Vogt. 2002. Tetraspan microdomains distinct from lipid rafts enrich select peptide-MHC class II complexes. *Nat. Immunol.* 3:61–68.

Larson, D.R., J.A. Gosse, D.A. Holowka, B.A. Baird, and W.W. Webb. 2005. Temporally resolved interactions between antigen-stimulated IgE receptors and Lyn kinase on living cells. *J. Cell Biol.* 171:527–536.

Le Naour, F., E. Rubinstein, C. Jasmin, M. Prenant, and C. Boucheix. 2000. Severely reduced female fertility in CD9-deficient mice. *Science.* 287:319–321.

Le Naour, F., M. Andre, C. Boucheix, and E. Rubinstein. 2006. Membrane microdomains and proteomics: lessons from tetraspanin microdomains and comparison with lipid rafts. *Proteomics.* 6:6447–6454.

Lenne, P.F., L. Wawrezinieck, F. Conchonaud, O. Wurtz, A. Boned, X.J. Guo, H. Rigneault, H.T. He, and D. Marguet. 2006. Dynamic molecular confinement in the plasma membrane by microdomains and the cytoskeleton meshwork. *EMBO J.* 25:3245–3256.

Levy, S., and T. Shoham. 2005. The tetraspanin web modulates immune-signalling complexes. *Nat. Rev. Immunol.* 5:136–148.

Ley, K., C. Laudanna, M.I. Cybulsky, and S. Nourshargh. 2007. Getting to the site of inflammation: the leukocyte adhesion cascade updated. *Nat. Rev. Immunol.* 7:678–689.

Little, K.D., M.E. Hemler, and C.S. Stipp. 2004. Dynamic regulation of a GPCR-tetraspanin-G protein complex on intact cells: central role of CD81 in facilitating GPR56-Galpha q/11 association. *Mol. Biol. Cell.* 15:2375–2387.

Luo, B.H., C.V. Carman, and T.A. Springer. 2007. Structural basis of integrin regulation and signaling. *Annu. Rev. Immunol.* 25:619–647.

Manly, B.F.J. 1997. Randomization, Bootstrap, and Monte Carlo Methods in Biology. Second edition. Chapman & Hall/CRC, London. 424 pp.

Miller, J., R. Knorr, M. Ferrone, R. Houdei, C.P. Carron, and M.L. Dustin. 1995. Intercellular adhesion molecule-1 dimerization and its consequences for adhesion mediated by lymphocyte function associated-1. *J. Exp. Med.* 182:1231–1241.

Min, G., H. Wang, T.T. Sun, and X.P. Kong. 2006. Structural basis for tetraspanin functions as revealed by the cryo-EM structure of uroplakin complexes at 6-A resolution. *J. Cell Biol.* 173:975–983.

Miyado, K., G. Yamada, S. Yamada, H. Hasuwa, Y. Nakamura, F. Ryu, K. Suzuki, K. Kosai, K. Inoue, A. Ogura, et al. 2000. Requirement of CD9 on the egg plasma membrane for fertilization. *Science.* 287:321–324.

Moseley, G.W. 2005. Tetraspanin-Fc receptor interactions. *Platelets.* 16:3–12.

Nydegger, S., S. Khurana, D.N. Krementsov, M. Foti, and M. Thali. 2006. Mapping of tetraspanin-enriched microdomains that can function as gateways for HIV-1. *J. Cell Biol.* 173:795–807.

Pileri, P., Y. Uematsu, S. Campagnoli, G. Galli, F. Falugi, R. Petracca, A.J. Weiner, M. Houghton, D. Rosa, G. Grandi, and S. Abrignani. 1998. Binding of hepatitis C virus to CD81. *Science.* 282:938–941.

Redford, G.I., and R.M. Clegg. 2005. Polar plot representation for frequency-domain analysis of fluorescence lifetimes. *J. Fluoresc.* 15:805–815.

Reilly, P.L., J.R. Woska Jr., D.D. Jeanfavre, E. McNally, R. Rothlein, and B.J. Bormann. 1995. The native structure of intercellular adhesion molecule-1 (ICAM-1) is a dimer. Correlation with binding to LFA-1. *J. Immunol.* 155:529–532.

Romero, I.A., C.L. Amos, J. Greenwood, and P. Adamson. 2002. Ezrin and moesin co-localise with ICAM-1 in brain endothelial cells but are not directly associated. *Brain Res. Mol. Brain Res.* 105:47–59.

Sachs, N., M. Kreft, M.A. van den Bergh Weerman, A.J. Beynon, T.A. Peters, J.J. Weening, and A. Sonnenberg. 2006. Kidney failure in mice lacking the tetraspanin CD151. *J. Cell Biol.* 175:33–39.

Sala-Valdes, M., A. Ursa, S. Charrin, E. Rubinstein, M.E. Hemler, F. Sanchez-Madrid, and M. Yanez-Mo. 2006. EWI-2 and EWI-F link the tetraspanin web to the actin cytoskeleton through their direct association with ezrin-radixin-moesin proteins. *J. Biol. Chem.* 281:19665–19675.

Sharma, P., R. Varma, R.C. Sarasij, Ira, K. Gousset, G. Krishnamoorthy, M. Rao, and S. Mayor. 2004. Nanoscale organization of multiple GPI-anchored proteins in living cell membranes. *Cell.* 116:577–589.

Simons, K., and D. Toomre. 2000. Lipid rafts and signal transduction. *Nat. Rev. Mol. Cell Biol.* 1:31–39.

Suzuki, K.G., T.K. Fujiwara, F. Sanematsu, R. Iino, M. Edidin, and A. Kusumi. 2007. GPI-anchored receptor clusters transiently recruit Lyn and G α for temporary cluster immobilization and Lyn activation: single-molecule tracking study 1. *J. Cell Biol.* 177:717–730.

Takeda, Y., I. Tachibana, K. Miyado, M. Kobayashi, T. Miyazaki, T. Funakoshi, H. Kimura, H. Yamane, Y. Saito, H. Goto, et al. 2003. Tetraspanins CD9 and CD81 function to prevent the fusion of mononuclear phagocytes. *J. Cell Biol.* 161:945–956.

Takeda, Y., A.R. Kazarov, C.E. Butterfield, B.D. Hopkins, L.E. Benjamin, A. Kaipainen, and M.E. Hemler. 2007. Deletion of tetraspanin Cd151 results in decreased pathologic angiogenesis in vivo and in vitro. *Blood.* 109:1524–1532.

Unternaehrer, J.J., A. Chow, M. Pypaert, K. Inaba, and I. Mellman. 2007. The tetraspanin CD9 mediates lateral association of MHC class II molecules on the dendritic cell surface. *Proc. Natl. Acad. Sci. USA.* 104:234–239.

van Buul, J.D., M.J. Allingham, T. Samson, J. Meller, E. Boulter, R. Garcia-Mata, and K. Burridge. 2007. RhoG regulates endothelial apical cup assembly downstream from ICAM1 engagement and is involved in leukocyte transendothelial migration. *J. Cell Biol.* 178:1279–1293.

Varma, R., and S. Mayor. 1998. GPI-anchored proteins are organized in submicron domains at the cell surface. *Nature.* 394:798–801.

Wouters, F.S., and A. Esposito. 2008. Quantitative analysis of fluorescence lifetime imaging made easy. *HFSP Journal*. 2:7–11.

Yan, Y., K. Shirakabe, and Z. Werb. 2002. The metalloprotease Kuzbanian (ADAM10) mediates the transactivation of EGF receptor by G protein-coupled receptors. *J. Cell Biol.* 158:221–226.

Yanez-Mo, M., A. Alfranca, C. Cabanas, M. Marazuela, R. Tejedor, M.A. Ursa, L.K. Ashman, M.O. de Landazuri, and F. Sanchez-Madrid. 1998. Regulation of endothelial cell motility by complexes of tetraspan molecules CD81/TAPA-1 and CD151/PETA-3 with α3 β1 integrin localized at endothelial lateral junctions. *J. Cell Biol.* 141:791–804.

Yanez-Mo, M., O. Barreiro, P. Gonzalo, A. Batista, D. Megias, L. Genis, N. Sachs, M. Sala-Valdes, M.A. Alonso, M.C. Montoya, et al. 2008. MT1-MMP collagenolytic activity is regulated through association with tetraspanin CD151 in primary endothelial cells. *Blood.* 112:3217–3226.

Yang, X., O.V. Kovalenko, W. Tang, C. Claas, C.S. Stipp, and M.E. Hemler. 2004. Palmitoylation supports assembly and function of integrin-tetraspanin complexes. *J. Cell Biol.* 167:1231–1240.

Yauch, R.L., and M.E. Hemler. 2000. Specific interactions among transmembrane 4 superfamily (TM4SF) proteins and phosphoinositide 4-kinase. *Biochem. J.* 351:629–637.

Zacharias, D.A., J.D. Violin, A.C. Newton, and R.Y. Tsien. 2002. Partitioning of lipid-modified monomeric GFPs into membrane microdomains of live cells. *Science.* 296:913–916.

Zhang, J., R.E. Campbell, A.Y. Ting, and R.Y. Tsien. 2002. Creating new fluorescent probes for cell biology. *Nat. Rev. Mol. Cell Biol.* 3:906–918.

Zhang, X.A., A.L. Bontrager, and M.E. Hemler. 2001. Transmembrane-4 superfamily proteins associate with activated protein kinase C (PKC) and link PKC to specific beta(1) integrins. *J. Biol. Chem.* 276:25005–25013.

Zhu, G.Z., B.J. Miller, C. Boucheix, E. Rubinstein, C.C. Liu, R.O. Hynes, D.G. Myles, and P. Primakoff. 2002. Residues SFQ (173-175) in the large extracellular loop of CD9 are required for gamete fusion. *Development.* 129:1995–2002.